

REDDENINGS, DISTANCES AND LUMINOSITIES

of a new sample of Galactic Cepheids for probing the Milky Way and calibrating
the extra-galactic distance scale

SHUBHAM MAMGAIN

Master Astrophysics

Matr. No. : 794731



SUPERVISOR I - Dr. Jesper Storm

Dwarf Galaxies and the Galactic Halo

Leibniz Institute for Astrophysics Potsdam (AIP)

SUPERVISOR II - Prof. Dr. Maria Rosa Cioni

Dwarf Galaxies and the Galactic Halo

Leibniz Institute for Astrophysics Potsdam (AIP)

Acknowledgement

To my teachers—who sparked insight within me, making visible to the mind what was invisible to the eyes—I offer my deepest gratitude.

I am especially thankful to my father, Dinesh Mamgain, who first introduced me to the power of mathematics as my personal tutor and has nurtured me with unwavering support to this day. My sincere thanks to Mayank Malhotra, a teacher, who revealed mathematics as a language of thought and inspired my pursuit of higher education. I am grateful to Dr. Taufiq Ahmed, whose teaching in statistical mechanics and electronics helped me transition from abstract thinking to the realm of physics.

I would like to thank Prof. Dr. Philipp Richter, who supported me generously, even beyond the academic setting in my master studies. I am also indebted to Prof. Martin Wendt, who guided my intuition on astronomical distance determination and mentored me in the development of scientific writing skills. Special appreciation goes to Prof. Dr. Achim Feldmeier, whose lectures in natural philosophy aligned my thinking with the clarity of scientific reasoning and deepened my understanding of mathematical modelling. I am also grateful to Dr. Jose Bogio, who gave me the opportunity to work as a lab assistant at AIP and introduced me to the practical world of lasers and on-chip spectrographs, building solid intuition on the physics of light. I am deeply indebted to Hendrik at KPMG Berlin, under whose guidance I gained practical experience and insight into data pipeline concepts—skills that have proven invaluable to this research.

This thesis would not have been possible without the invaluable mentorship of Dr. Jesper Storm, my master thesis supervisor—the most humble person I have ever met—under whose guidance I elevated my understanding from theoretical concepts to astronomical applications. I am equally grateful to Prof. Maria-Rosa L. Cioni, my secondary thesis supervisor, whose openness and organisation support helped me navigate the learning process with confidence. My sincere gratitude to Dr. Barry Madore for the valuable communication on the research topic, as his scientific work served as the basis of this research thesis.

I am also deeply grateful to my friends, who each contributed to this journey in their own meaningful way. Their companionship, encouragement, and insight have been a constant source of strength.

I thank Pankaj Negi for fostering an intellectually rich environment during my formative years. I am grateful to Marco Floris and Mattia Toffano for accompanying me as close friends during the early days of my studies abroad. My heartfelt thanks to Selina Syed, Jakob Drews, Merlin Wagner, Jan Vincent and Maximilian Ueberschar for their unwavering support, which has felt as comforting and constant as that of family. I also thank Kuan Yu, Luzie Frietag, Aaraw Rauniyar, Chryssi Tzagkarakis, Partha Pritam Das, Ravi Shankar Chaurasia, Theodor Mc Carthy and Dipesh Sosa for cultivating an academic space where open intellectual discourse flourished, enriching our understanding of interdisciplinary concepts. And finally, to Joy Krecke, for sharing wisdom and offering a broader perspective on perception and communication. Together, over time, their presence in my life has deeply influenced my interdisciplinary learning and continuously inspired me to seek a deeper understanding of this existence.

Above all, I owe my deepest love and gratitude to my mother, Geeta Mamgain, whose unwavering devotion, quiet strength, and constant belief in me have been the foundation of everything I have achieved. Her nurturing presence and endless support played a profound role in shaping my self-confidence and determination. This work stands as much on her sacrifices as it does on my efforts.

Shubham Mamgain

Potsdam, 2025

Abstract

Aim: Calibration of BVIJHK Galactic Leavitt Law by determining systematic errors in reddening and distance of individual Cepheids.

Method: Inspired by Madore's (2017) Leavitt Law calibration algorithm, this research compares the systematic errors yield by four versions of Wesenheit functions based on (B-J), (B-K), (V-J) and (J-K) color indices. Starting with residual correlation of period-luminosity relations with period-wesenheit relations, bandwise extinction error for given distance moduli trails being calculated for each of the four cases. Distance error trail with the least variance in reddening error across the bands selected as the systematic error pair and adjusted to the luminosities. Calibration with (B-K) and (V-J) based wesenheit yields the tightest Leavitt Law for all the bands. The results demonstrate improved internal consistency in the near-infrared bands and contribute to a more precise calibration of the extragalactic distance scale—thus reinforcing the reliability of the cosmic distance ladder as a tool for precision cosmology.

Result: The calibrated BVIJHK Leavitt Laws using 95 Galactic Cepheids are as follows.

Leavitt Law: BK based

$$\begin{aligned} M_B &= -1.86(\log P - 1)(\pm 0.011) - 3.22(\pm 0.003) \\ M_V &= -2.26(\log P - 1)(\pm 0.003) - 3.95(\pm 0.001) \\ M_I &= -2.57(\log P - 1)(\pm 0.014) - 4.74(\pm 0.004) \\ M_J &= -2.79(\log P - 1)(\pm 0.011) - 5.22(\pm 0.003) \\ M_H &= -2.92(\log P - 1)(\pm 0.011) - 5.60(\pm 0.003) \\ M_K &= -2.97(\log P - 1)(\pm 0.011) - 5.65(\pm 0.003) \end{aligned}$$

Leavitt Law: VJ based

$$\begin{aligned} M_B &= -1.85(\log P - 1)(\pm 0.009) - 3.22(\pm 0.003) \\ M_V &= -2.26(\log P - 1)(\pm 0.010) - 3.95(\pm 0.003) \\ M_I &= -2.56(\log P - 1)(\pm 0.018) - 4.73(\pm 0.005) \\ M_J &= -2.78(\log P - 1)(\pm 0.010) - 5.22(\pm 0.003) \\ M_H &= -2.92(\log P - 1)(\pm 0.014) - 5.60(\pm 0.004) \\ M_K &= -2.97(\log P - 1)(\pm 0.014) - 5.65(\pm 0.004) \end{aligned}$$

VIJK Leavitt Law calibrated with (V-J) based wesenheit yields the distances to LMC and SMC as 18.378 ± 0.114 and 19.070 ± 0.032 , respectively.

Contents

Acknowledgements	ii
Abstract	iii
List of Figures	vi
List of figures	viii
List of Tables	ix
List of tables	ix
1 Introduction	1
1.1 Prespective on the Subject	1
1.1.1 Astrophysics, Astronomy and Cosmology	1
1.1.2 Spectrum of Spatial Scale	2
1.2 Historical Background and Development	5
1.2.1 Distance Determination beyond the Galaxy, 1920s	6
1.2.2 Expansion of the Universe	7
1.2.3 The Big Bang Model, 1930s	7
1.2.4 Composition of Stars	8
1.2.5 Age of the Universe, 1950s	8
1.2.6 Technological Development, 1960s	9
1.2.7 Golden Era of Astronomy - Gaia onwards	9
1.3 Scope of this Thesis	10
1.3.1 Part I: Parameters of Leavitt Law	10
1.3.2 Part II: Calibration Method and Dataset	11
1.3.3 Result Implications	11
I Parameters of Leavitt Law	15
2 Observables - Luminosity, Reddening, Distance	16

2.1	Why does a star shine?	16
2.2	Light: Color and Luminosity	17
2.2.1	Magnitude Scale	18
2.2.2	Color Index ($m_1 - m_2$)	19
2.2.3	Absolute Magnitude (M)	20
2.3	Distance	21
2.3.1	Parallax: Measuring Astronomical Distances Using Geometry	21
2.3.2	Distance Modulus (μ)	22
2.4	Interstellar Reddening	23
2.4.1	Reddening Ratio	23
2.4.2	Interstellar Extinction Law	24
2.4.3	Wesenheit Magnitude	25
3	Pulsating Star - Classical Cepheid	28
3.1	Are all stars the same?	28
3.1.1	Discovery of Variable stars	28
3.2	Color-Magnitude Diagram	29
3.2.1	Spectral Classification	29
3.2.2	Stellar Evolution	29
3.3	Pulsation of Cepheid	36
3.3.1	Kappa Mechanism	36
3.4	Leavitt Law	37
II	Calibration Method and Dataset	39
4	Calibration Method	40
4.1	Galactic Cepheid Dataset	40
4.2	Leavitt Law and their Wesenheits	40
4.3	Residual Analysis	42
4.4	Decoupling $\delta\mu - \delta E_{BV}$	45
4.5	Calibrated Leavitt Law	48
4.6	cluster Cepheid	49
5	Discussion	50
5.1	Reddening Comparison	50
5.2	Distance Comparison	50
5.3	Luminosity Comparison	50

5.4	Effect of Metallicity	50
6	Conclusion	51
6.1	Result	51
6.2	Application Of The Result	51
	Bibliography	53
	Bibliography	54

List of Figures

1.1	Cosmic distances span from nearby stars to the largest known structures in the universe, measured on scales of light-years, typically up to the order of 10. Each label represents either the distance to a notable astronomical object or the size of a vast cosmic region. The diameter of the observable universe is roughly 93 billion light-years, which is nearly the order of 11.	2
1.2	<i>Left:</i> Stars located within 15ly. <i>Right:</i> A segment of the Milky Way depicting the Solar System and its neighboring nebulae located in the Orion–Cygnus Arm. The Galactic Center and other minor arms - Norma and Carina–Sagittarius - are also highlighted.	3
1.3	<i>Left:</i> Side view of the Milky Way, depicting its components and satellite galaxies, notably the Large and Small Magellanic Clouds (LMC and SMC). <i>Right:</i> Spatial distribution of galaxies within the Local Group, dominated by the Milky Way and Andromeda galaxies. Source: Wikipedia - Pablo Carlos Budassi (left) and Andrew Z. Colvin (right)	4
1.4	Galaxy supercluster and voids within 10^9 ly of Virgo Supercluster. Source: Andrew Z. Colvin (Wikipedia)	4
1.5	Large-scale structure of the Universe illustrating the cosmic web. <i>Source:</i> S. Stabelberg, <i>Structures blog from the University of Heidelberg</i>	6
1.6	Two remarkable discoveries of early twentieth century: a) Leavitt Law: Period (in logarithmic scale) of 25 Cepheids (of Small Magellanic Cloud) correlated with their maximum and minimum brightness. Leavitt and Pickering (1912) b) Hubble Law: Increasing recession velocity of galaxies with respect to distance suggesting an expanding Universe. Hubble (1929)	7
1.7	<i>K-band Period-Luminosity relation for Galactic Cepheid using IRSB distance.</i> Source: Storm J., 2011	10
1.8	The fractional composition of the Universe consists of dark energy (68 %), dark matter (27 %), and baryonic matter (5 %) is depicted, with the contributions from radiation and other relativistic particles neglected.	12

1.9 An instance of Cosmic Distance Ladder calibrating Leavitt Law with parallax, SNIa with Leavitt Law and Hubble Law with SNIa based distances. (Riess et al., 2022)	13
2.1 <i>Black body radiation curves based on Planck's Law for various temperatures. The maxima of the curves shift according to Wien's displacement law. Source: Wikipedia commons</i>	17
2.2 As Earth orbits the Sun, nearby stars appear to shift against distant background stars—this shift, called parallax, is used to measure their distance using trigonometric ratio. <i>Source: hyperphysics.phy-astr.gsu.edu</i>	22
2.3 Comparision between emitted (0) and observed (1) SEDs. For given band, deviation between the curves represents interstellar extinction (here, A_B and A_V). On the right side, the relative difference between extinction of two bands depicting the definition of interstellar reddening $E(B - V)$. (Krelowski and Papaj, 1993)	23
2.4 Galactic extinction law fitted for UBRIJHKL along three directions in the sky, with varying R_V , with A_V as reference. (Cardelli et al., 1989)	24
3.1 Evolutionary cycle for low and high mass star. Low mass stars, like Sun, become a Red Giant when Hydrogen supply to the core stops and fusion takes place in the shell around the core. Afterwards they become a Planetary nebula with a bright core at the center and end their life as a White Dwarf, slowly get faded turning into brown dwarf. Massive stars evolve to Red Supergiant and end their life as Supernova leaving behind either a Neutron star or Black Hole. [cmglee/NASA Goddard Space Flight Center]	30
3.2 Following proton-proton fusion, accumulation of Deuterium opens possibility for fusing with one more proton to form Helion - an isotope of Helium with two protons and one neutron. Rising temperature fuses two Helion atoms to form Helium (two protons and two neutrons) which is a stable element and emits two Hydrogen atoms. This series of reactions from Hydrogen to Helium is called p-p chain (pp I branch) reaction. Other rarer reactions can also occur inside the star. For instance, pp II branch when Helion fuses with Helium to form Beryllium (4 protons and 3 neutron). then either Beryllium decays to Lithium (3 protons and 4 neutron), Lithium fuses with proton and breakdown into two Helium atoms. In pp III branch, Beryllium fuses with proton to form Boron (4 proton and 4 neutron) which is unstable, breaking down into Helium. The most rare case is pp IV branch, when Helion captures a proton and form Helium. All these four branches are called pp chain reaction. Source: F. Reines, Ann. Rev. Nucl. Sci. 10 (1960) 1-26	30

3.3	Isochrones of stars with different masses depicting their evolutionary traids. Massive stars not Source: Universe (VIII edition) by Roger A. Freedman & William J. Kaufmann III	32
3.4	Stellar Evolution of Sun-type star: a) Gravitational collapse of a gas cloud forms a protostar which begin to fuse Hydrogen and arrived to the main sequence. b) After billions of years, star leaves the main sequence and become a Red Giant. At the tip of the Red Giant branch, star begin to fuse Helium after the episode of Helium flash and slowly moves to AGB phase c) Evolved star expanded upto the size of Jupiter orbit and loses its envelope to form a planetary nebula at the age of 12 billion years. d) Ejecting way the outer envelope, the remnant of dead star shines due to the degeneracy pressure of its electron and called as White Dwarf. Source: Stars and Nebula by William J. Kaufmann, III	35
4.1	103 Galactic Cepheids BVIJHK photometric data with color excess (E_{BV}) and Gaia distance (RUWE < 1.4). No clear correlation with period is observed in any of the pairplot.	40
4.2	BVIJHK PL and PW relations with their Pearson correlation coefficient (r-value) . . .	41
4.3	Slope and Intercept of BVIJHK PL and PW relations. Interestingly, PW seems constant for all the bands, which is not the case for PL relations.	42
4.4	$\Delta W - \Delta M$ correlation plots shown for three versions of wesenheit - VI and JK. With increasing wavelength, slope is approaching to 1.	43
4.5	For each star, multiple trials are conducted to estimate the reddening-distance error pair in the B band. This process is then repeated for the remaining bands to constrain the correct $\delta\mu - \delta E_{BV}$ error pair. Madore et al. (2017)	44
4.6	Determination of reddening error with least variance over modulus error for four family of wesenheit function. Dashed blue line depicts the variance.	47
4.7	BVIJHK PL and PW relations with their Pearson correlation coefficient (r-value) . .	48
4.8	BVIJHK PL and PW relations with their Pearson correlation coefficient (r-value) . .	49

List of Tables

2.1	Conversion of Astronomical Distance Units	21
2.2	Extinction Law and corresponding reddening ratio adopted from Table 4 of Fouqué et al. (2007)	25
4.1	PL relations are shown in six bands, along with the corresponding PW relations in four colors. Notice the decreasing error in the slope and intercept with increasing wavelength.	40
4.2	Slopes of residual correlation $\Delta W_{\lambda}^{12} - \Delta M_{\lambda}$ for BI, VI, IH and JK. Note the systematic decrease in errors as the slope ρ approaching to 1 with increasing wavelength.	45

1 Introduction

Who really knows?
Who will unfold it?
How did this Universe formed?
Where does it come from?
Gods came after the creation.
Then, who really witnessed the
origin of this existence?

Rigved X.129.6

1.1 Prespective on the Subject

Have you ever wondered why the Sun shines, why stars exhibit different colors, or what the structure of the Milky Way is? How far is the Andromeda galaxy from Earth? Do structures larger than galaxies exist? How far into the Universe can we observe? And perhaps most intriguingly, are we alone in this vast cosmos?

1.1.1 Astrophysics, Astronomy and Cosmology

Such fundamental questions have been explored—though not yet fully answered—through the field of astrophysics. By observing the Universe across vast distances and in all directions using various wavelengths and observational techniques, scientists have begun to unravel these cosmic mysteries. Astrophysics is inherently interdisciplinary, drawing upon principles from physics, chemistry, geology, computer science, and other fields to construct a coherent understanding of the Universe and our place within it. Astrophysicists investigate the interactions and evolution of celestial bodies, the dynamics of cosmic ecosystems, and the potential existence of extraterrestrial life.

Astronomy can be regarded as the precursor to astrophysics, focusing on the study of the positions, motions, brightness, and classifications of celestial objects. This observational approach is essential for modeling the dynamics of the Universe, allowing us to predict astronomical events such as solar and lunar eclipses, planetary conjunctions, stellar motion within the Galaxy, and to map the observable Universe. In essence, astronomy addresses "what" and "where" questions, while

astrophysics delves into "how" and "why" inquiries.

On a broader scale, cosmology treats the Universe as a unified system. It explores the shape, age, evolution, and ultimate fate of the Universe. In examining the vast spectrum of spatial scales, galaxies appear as the fundamental units, organized into larger structures such as galaxy clusters and superclusters, all interconnected by cosmic filaments of gas and dark matter. These large-scale structures collectively form the cosmic web.

Constrained by observational data, cosmology is closely aligned with philosophical inquiry and stands as one of the oldest scientific fields studied by humanity.

1.1.2 Spectrum of Spatial Scale

The hymns of Rigved, originally composed in Sanskrit over 2,500 years ago, remain strikingly relevant to modern cosmology. They reflect a deep philosophical inquiry into the origins, scales and structure of the Universe—an inquiry that continues today as our understanding evolves through ongoing observation and theoretical advancement. In this section, I provide a brief overview of the Universe's structure as revealed by contemporary astronomical observations.

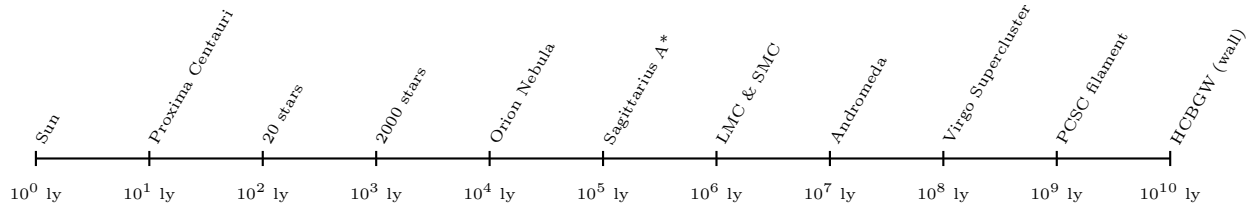


Figure 1.1: Cosmic distances span from nearby stars to the largest known structures in the universe, measured on scales of light-years, typically up to the order of 10. Each label represents either the distance to a notable astronomical object or the size of a vast cosmic region. The diameter of the observable universe is roughly 93 billion light-years, which is nearly the order of 11.

Milky Way in Perspective

To gain perspective on the size of the Universe, it is useful to compare distances across different scales. For instance, the nearest star to the Sun is Proxima Centauri, located approximately 4.24 light-years away. By definition, one light-year is the distance that light travels in a vacuum over the course of one year, equivalent to approximately 9.46 trillion kilometers. Within a 10 light-year radius of the Sun, there are about 20 stars, and nearly 2,000 stars lie within 100 light-years. The stars of the Orion Belt are situated at distances ranging from 800 to 1,300 light-years.

The Milky Way Galaxy is characterized by three major spiral arms—Perseus, Scutum-Centaurus, and Sagittarius—and three minor arms: the Orion Spur, Carina-Sagittarius, and Norma Arms. Our Solar System is located within the Orion Spur, a region containing millions of stars, situated between the Perseus Arm on the inner side and the Scutum-Centaurus Arm on the outer side.

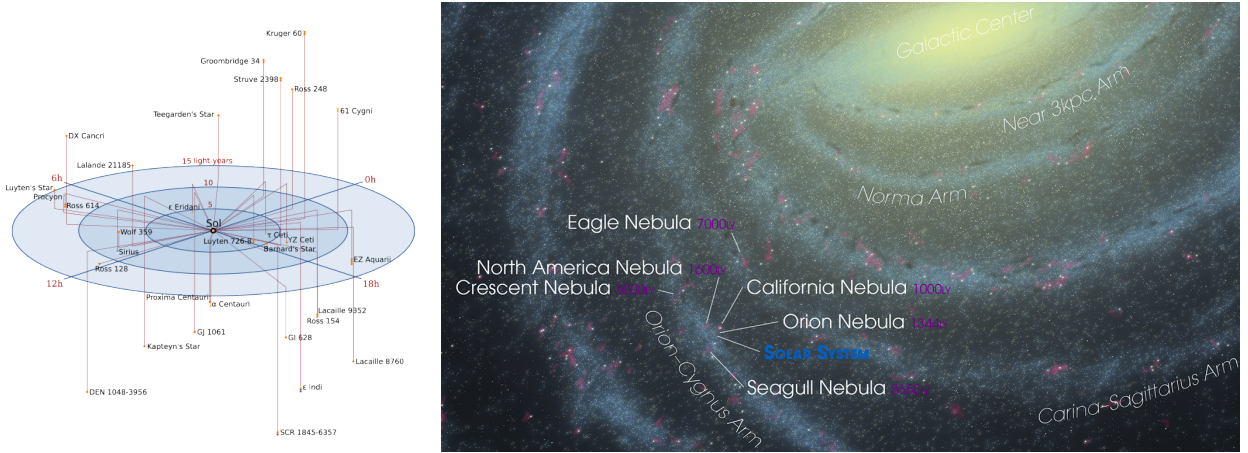


Figure 1.2: *Left:* Stars located within 15ly. *Right:* A segment of the Milky Way depicting the Solar System and its neighboring nebulae located in the Orion–Cygnus Arm. The Galactic Center and other minor arms - Norma and Carina–Sagittarius - are also highlighted.

The Perseus and Scutum-Centaurus arms seem to converge near the ends of the Long Bar, a stellar structure that stretches roughly 15,000 light-years and extends through the Galactic center. At the galaxy's core lies Sagittarius A*, a supermassive black hole believed to be the rotating nucleus of the galaxy. It is located approximately 27,000 light-years from Earth. Collectively, these elements contribute to the Milky Way's characteristic spiral disk structure, with a prominent bulge at its center.

Galactic Halo and Galaxies around

The Milky Way's spiral structure spans roughly 100,000 light-years in diameter, and is surrounded by a spherical halo extending up to three times that size. This halo hosts numerous satellite galaxies. One of the most prominent and easily visible from the southern hemisphere is the Large Magellanic Cloud (LMC), the Milky Way's largest satellite galaxy, located about 160,000 light-years (50 kpc) away. The LMC itself has a satellite—the Small Magellanic Cloud (SMC)—located approximately 200,000 light-years (60 kpc) from Earth. In total, the Milky Way has over 50 known satellite galaxies. Its nearest large galactic neighbor is the Andromeda Galaxy (M31), situated around 2.54 million light-years (778 kpc) away. Andromeda is roughly two to three times larger than the Milky Way.

Expanding the view to a radius of 10 million light-years, the region contains about 56 galaxies, among which the Milky Way and Andromeda are the most massive and gravitationally dominant. This collective of galaxies is known as the Local Group, which itself resides in the central region of the Virgo Supercluster.

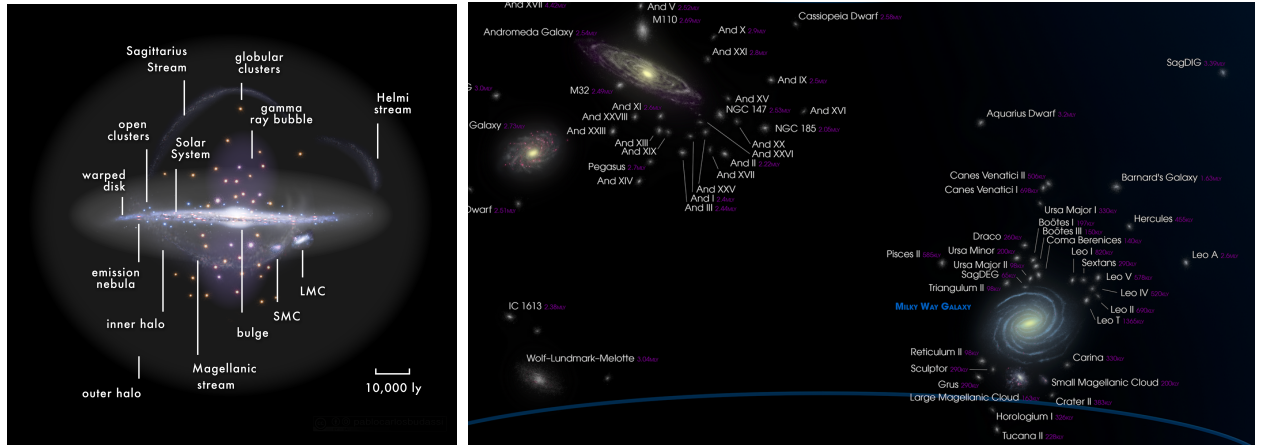


Figure 1.3: *Left:* Side view of the Milky Way, depicting its components and satellite galaxies, notably the Large and Small Magellanic Clouds (LMC and SMC). *Right:* Spatial distribution of galaxies within the Local Group, dominated by the Milky Way and Andromeda galaxies. Source: Wikipedia - Pablo Carlos Budassi (left) and Andrew Z. Colvin (right)

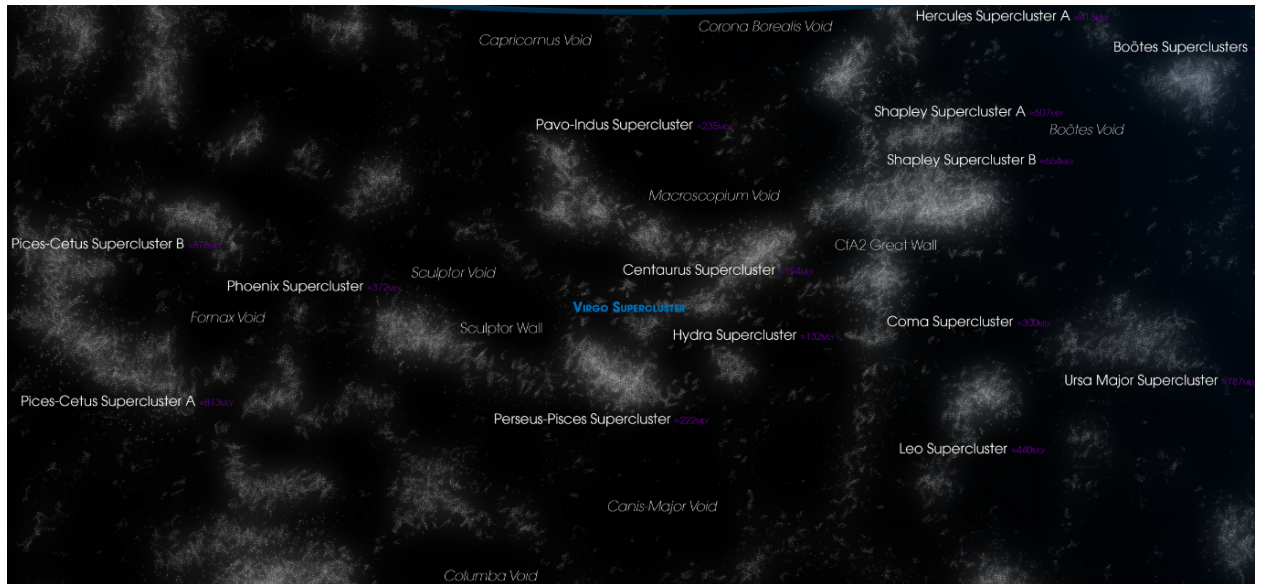


Figure 1.4: Galaxy supercluster and voids within 10^9 ly of Virgo Supercluster. Source: Andrew Z. Colvin (Wikipedia)

Galaxy Clusters to Superclusters

As we consider larger cosmic scales, the megaparsec (Mpc) becomes a more convenient unit for measuring distances. One megaparsec is approximately 3.26 million light-years. The Virgo Supercluster, which includes the Local Group, the Virgo Cluster, and several other galaxy clusters, spans a diameter of about 33 Mpc (roughly 100 million light-years).

The Virgo Supercluster is situated within the Laniakea Supercluster, a much larger structure that encompasses a volume about five times greater and contains approximately 100,000 galaxies. Other major regions within Laniakea include the Pavo-Indus Supercluster, the Southern Supercluster, and the Hydra-Centaurus Supercluster.

At the heart of Laniakea, within the Hydra-Centaurus Supercluster, lies a region of maximum gravitational attraction known as the Great Attractor. Most galaxies within Laniakea—including the Milky Way—are being gravitationally drawn toward this region.

Cosmic Web: Filaments, Walls and Voids

The Laniakea Supercluster, along with the Shapley, Hercules, Coma, and Perseus–Pisces Superclusters, are all part of a vast galactic filament known as the Pisces–Cetus Supercluster Complex (PCSC). This structure is estimated to be approximately 1 billion light-years long and 150 million light-years wide, making it one of the largest known structures in the observable Universe.

Adjacent to it lies an even slightly larger filament known as the Perseus–Pegasus Filament. However, the largest known galaxy filament is the Hercules–Corona Borealis Great Wall (HCBGW), which stretches up to 10 billion light-years in length—roughly one-tenth the diameter of the observable Universe. Billions of such galaxy filaments, interwoven with gigantic cosmic voids, form the cosmic web—a vast, interconnected structure that defines the large-scale architecture of the Universe. This grand-scale pattern of matter distribution is illustrated in Figure 1.5.

1.2 Historical Background and Development

Advancements in observational technology have enabled the exploration of the Universe at unprecedented depths and resolutions. These technological developments have profoundly influenced our understanding, offering novel perspectives on the evolutionary history and large-scale structure of the cosmos. This section presents a concise overview of the historical progression of astronomical research, with particular emphasis on pivotal discoveries and theoretical developments made over the past century that have fundamentally shaped contemporary cosmology.

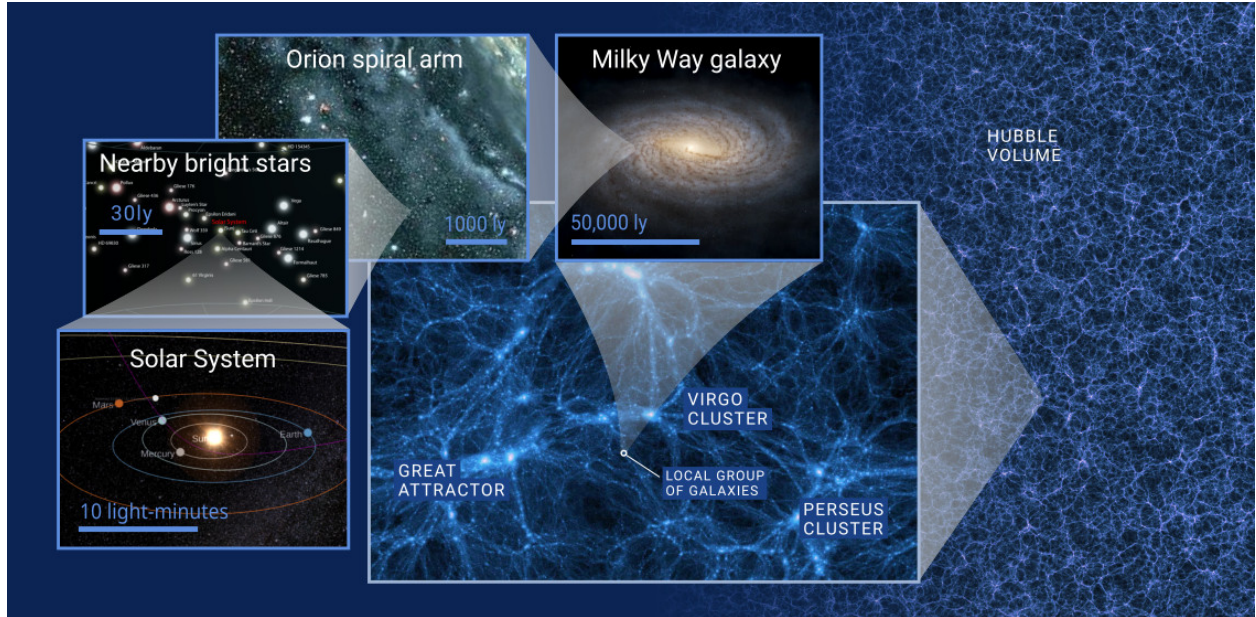


Figure 1.5: Large-scale structure of the Universe illustrating the cosmic web. *Source: S. Stapelberg, Structures blog from the University of Heidelberg*

1.2.1 Distance Determination beyond the Galaxy, 1920s

Prior to the twentieth century, the Milky Way (MW) was widely regarded as the entirety of the Universe, believed to be approximately 1.8 billion years old. The Sun was thought to occupy the central position in the cosmos, while other galaxies were misidentified as localized gaseous clouds within the Milky Way, and were classified as *spiral nebulae*. This fundamental misunderstanding regarding the scale of the Universe led to a protracted debate among astronomers, most notably the Shapley–Curtis Debate in 1920, between Harlow Shapley and Heber Curtis.

A key issue underlying this debate was the inability to accurately determine the distances to these spiral nebulae. The breakthrough came with the discovery of the period–luminosity relation for pulsating stars—specifically, Cepheid variables—by Henrietta Swan Leavitt in 1912 (Leavitt, 1908; Leavitt and Pickering, 1912). Her empirical relation, expressed as $m_{max} \propto \log P$, enabled astronomers to estimate extragalactic distances with far greater accuracy. This development proved instrumental in resolving the scale of the Universe and is illustrated in Figure 1.6.

Note 1.2.1: Knowledge of Distance is fundamental in astronomy.

Distance enables us to convert the sky's seemingly two-dimensional projection into a three-dimensional representation of the Universe. Once the distance to a bright object is known, its true luminosity can be determined, allowing us to infer its size, mass, age and other physical characteristics.

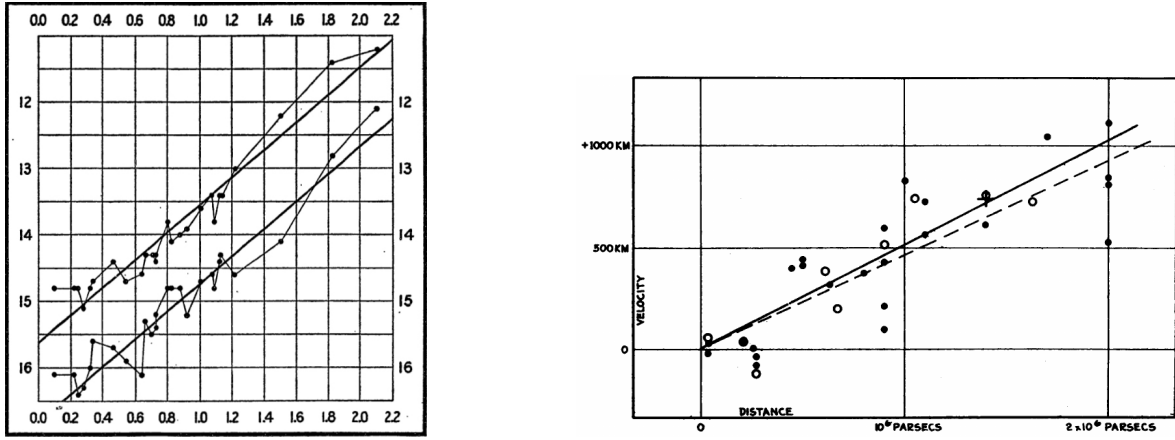


Figure 1.6: Two remarkable discoveries of early twentieth century: a) Leavitt Law: Period (in logarithmic scale) of 25 Cepheids (of Small Magellanic Cloud) correlated with their maximum and minimum brightness. [Leavitt and Pickering \(1912\)](#) b) Hubble Law: Increasing recession velocity of galaxies with respect to distance suggesting an expanding Universe. [Hubble \(1929\)](#)

1.2.2 Expansion of the Universe

In 1923, using the most advanced instrument of his time, the 100 - inch (2.5 m) Hooker Telescope, Edwin Hubble observed the Andromeda *spiral nebula* (M31) and successfully resolved a Cepheid variable star within it. By applying the Leavitt Law (period-luminosity relation) ([Hubble, 1925](#)), he estimated the distance to M31 and demonstrated that it lay far outside the boundaries of the Milky Way. This discovery effectively resolved the "Great Debate" in favor of Heber Curtis, confirming that Andromeda is a separate galaxy, and that the Milky Way is just one of billions of galaxies in the Universe.

Continuing his observations of Cepheid variables, Hubble measured distances to additional galaxies and identified a key relationship: the recessional velocity of a galaxy increases with its distance from the observer, expressed as $v \propto D$ ([Hubble, 1929](#)); see Figure 1.6. This empirical relation, now known as Hubble's Law, led to the revolutionary conclusion that the Universe is expanding in all directions - a concept that contradicted Einstein's earlier static model of the Universe ([Einstein, 1917](#)). The constant of proportionality in this relation, known as the Hubble constant H_0 , is of great cosmological importance, as it provides a measure of the expansion rate and thus the age of the Universe.

1.2.3 The Big Bang Model, 1930s

In the meantime, building upon Einstein's theory of general relativity, Georges Lemaître independently arrived at the conclusion of an expanding Universe, and proposed that its earliest state was an immensely hot and dense origin ([Lemaître, 1931](#)). Further theoretical advances were made in 1948, when Alpher and Herman ([Alpher and Herman, 1948](#)) refined Gamow's model of the early Universe

(Gamow, 1948) and predicted the existence of cosmic microwave background (CMB) radiation—a thermal remnant of the Big Bang - at a temperature of approximately 5K.

This prediction was confirmed in 1965, when Arno Penzias and Robert Wilson detected microwave radiation with a temperature of $3.4 \pm 1\text{K}$ using the Holmdel Horn antenna (Penzias and Wilson, 1965). Their discovery provided strong empirical support for the Big Bang model, which today stands as the standard cosmological model, describing the origin, evolution, and large-scale structure of the Universe.

1.2.4 Composition of Stars

Parallel advancements in quantum physics during the early twentieth century significantly enhanced our understanding of stellar evolution. In 1917, Arthur Eddington proposed a thermodynamic model based on free radial oscillations to explain the pulsations observed in Cepheid variable stars (Eddington, 1917). Building on this framework, he hypothesized in 1920 that the primary source of stellar energy is hydrogen fusion into helium (Eddington, 1920)—a revolutionary idea at the time.

Further insights emerged from the study of stellar spectra. In her 1925 Ph.D. dissertation, Cecilia Payne (later Payne-Gaposchkin) demonstrated that hydrogen and helium are the most abundant elements in stars, contradicting the prevailing view that stars had compositions similar to Earth (Payne-Gaposchkin, 1925). Her groundbreaking work established these two elements as the principal constituents of stellar matter. A comprehensive theoretical account of nuclear fusion reactions within stars was later formulated by Hans Bethe in 1939 (Bethe, 1939), laying the foundation for modern stellar nucleosynthesis theory. It was a major leap in astronomy, as the physics of internal mechanics of stars was not well known prior, including the right mechanism behind the cyclic pulsation of Cepheid variable.

1.2.5 Age of the Universe, 1950s

Studying stellar pulsations, Walter Baade discovered that Cepheid variables are divided into two distinct populations: Type I (classical Cepheids), which are brighter, and Type II (W Virginis stars). His recalibration of the Cepheid distance scale led to a doubling of the estimated distance to the Andromeda Galaxy and a corresponding revision of the Universe's age from 1.8 billion to 3.6 billion years (Baade, 1958). This estimate was further refined by his student, Allan Sandage, who extended Leavitt's relation into a period–color–luminosity law and revised the Hubble constant to 75 km/s/Mpc in 1958 (Sandage, 1958), resulting in an updated estimate of the age of the Universe at approximately 14 billion years. Allan's estimation lies near to modern value of Hubble constant.

1.2.6 Technological Development, 1960s

Despite numerous unresolved questions and theoretical challenges, technological advancements have significantly propelled research in astronomy, leading to major breakthroughs and providing deeper insights into the nature and evolution of the Universe. Beginning in the 1960s, the introduction of digital imaging in photometry revolutionized observational astronomy. The replacement of photographic plates with charge-coupled device (CCD) cameras markedly improved the accuracy, sensitivity, and precision of photometric measurements.

The deployment of space-based telescopes enabled observations across the entire electromagnetic spectrum, overcoming the limitations imposed by Earth's atmosphere on ground-based instruments. Additionally, the detection of cosmic rays, neutrinos, and gravitational waves opened new avenues for studying celestial phenomena through multiple independent messengers, thereby giving rise to the field of *multimessenger astronomy*. Concurrently, advances in high-energy particle physics uncovered the quantum-scale substructure of matter, contributing to more refined and physically grounded models of astrophysical processes. Collectively, these technological and theoretical developments have brought a paradigm shift in our understanding of the cosmos, marking the onset of what is often referred to as the golden era of modern astronomy.

One of the major development comes from Hubble Space Telescope (HST) key projects, especially key project I

1.2.7 Golden Era of Astronomy - Gaia onwards

The launch of the Gaia satellite by the European Space Agency (ESA) in 2013 marked a significant leap in modern astronomy. Utilizing the geometric parallax method with the baseline of Earth's orbital diameter, Gaia has precisely measured the distances to over 1.8 billion stars within the Milky Way and its surrounding regions, while simultaneously conducting extensive photometric and astrometric observations of the sky. The exceptional accuracy of Gaia's measurements has established a new standard for distance calibration in astronomical research. This research work relies on distance measurements obtained from the parallax data of Gaia Data Release 3 (DR3).

In 2021, the launch of the James Webb Space Telescope (JWST) by NASA further advanced the observational capabilities. With its sensitivity to the far-infrared spectrum, JWST has begun to reveal unprecedented details of the early Universe, including the formation of the first galaxies and stars. In addition to these missions, a number of major cosmological surveys and observatories—such as SDSS, Planck, and 2dFGRS—have already made transformative contributions to our understanding of the cosmos. Looking ahead, the commissioning of next-generation facilities, including the Vera C. Rubin Observatory, DESI, 4MOST, Euclid, SKA, and LISA, is expected to redefine the frontiers of observational astronomy and cosmology, setting new benchmarks for future research.

1.3 Scope of this Thesis

The aim of this thesis is to improve the accuracy of Galactic Leavitt Law - a primary distance indicator of cosmic distance ladder. Note the large scatter in linear period-luminosity relation of Cepheids, giving uncertainty to the slope and zero point of the fit. Using such a period-luminosity relation as a reference for the next rung of distance scale leads to larger error in the measurements, making it crucial to have a tight PL relation in the first place - to gain a high confidence on the cosmological scale studies. To refine the Leavitt Law to its finest form, I will be taking following steps which will be briefly discussed in following chapters.

- Identify and omit the outliers from BVIJHK photometric dataset of Galactic Cepheid.
- Estimate intrinsic luminosity of observed targets using reddening and Gaia DR3 parallax.
- Determine error in distances and interstellar reddenings following the method of [Madore et al. \(2017\)](#).
- Reformulate the Leavitt Law with distance-reddening corrected intrinsic luminosity of Cepheids.
- Cross validate the calibrated Leavitt Law with Cluster Cepheid based Leavitt Law.
- Apply the refined Leavitt Law on LMC and SMC Cepheids to determine their distances.

1.3.1 Part I: Parameters of Leavitt Law

The period-luminosity scatter plot requires primarily two parameters of Cepheid variables: a) accurate measurement of pulsation period, and b) accurate estimation of intrinsic luminosity of the respective Cepheid star. The Figure 1.7 depicts an instance of Leavitt Law in K band, where distances to individual stars measured by infrared surface brightness (IRSB) method ([Storm et al., 2011](#)), and interstellar extinction derived using Fouque's extinction law ([Fouqué et al., 2007](#)) and Fernie's reddening measurements ([Fernie, 1994](#)).

The pulsation periods of Cepheid variables are determined from light curves based on photometric observations spanning multiple pulsation cycles. This parameter is well-constrained for all Cepheid targets considered in this study. The primary focus of this research, however, lies in determining the second essential quantity—the intrinsic (absolute) luminosity of these stars. While telescopes measure the apparent luminosity, estimating the absolute luminosity requires correcting for both the distance the light has traveled and the attenuation caused by interstellar extinction.

Stellar light is subject to scattering and absorption as it traverses the interstellar medium, partic-

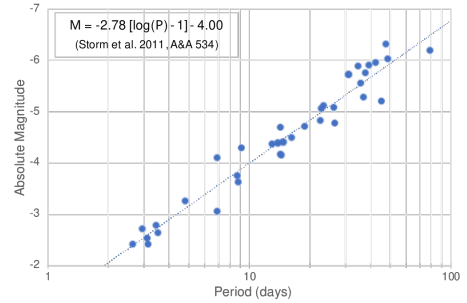


Figure 1.7: *K*-band Period-Luminosity relation for Galactic Cepheid using IRSB distance. Source: Storm J., 2011

ularly through dust and gas clouds along the line of sight. Any imprecision in correcting for these effects leads to significant deviations from the expected linear relationship in the period-luminosity relation. Consequently, accurately quantifying the uncertainties in distance and interstellar reddening for each Cepheid is a central objective of this thesis.

The first part of this thesis is dedicated to a detailed examination of these parameters and their interdependencies, as outlined in the next chapters.

1.3.2 Part II: Calibration Method and Dataset

This part of thesis contains three chapters covering details on Galactic Cepheid dataset, calibration methodology, its related physics and comparision plots. The Galactic Cepheid dataset used in this thesis contains multiband photometric data in the BVIJHK bands. The extinction law developed by Cardelli et al. ([Cardelli et al., 1989](#)), in combination with the total-to-selective extinction ratio adopted from Sandage ([Sandage et al., 2004](#)), is employed to convert the color excess values compiled by Fernie into BVIJHK extinction. Using parallactic distance estimates from the Gaia mission and extinction, raw Leavitt Law are derived.

The calibration technique used in this thesis is devised by Barry Madore ([Madore et al., 2017](#)). Utilizing the reddening-free nature of the Wesenheit function ([Madore, 1982](#)), the effect of reddening and distance errors on individual Cepheid can be decoupled and traced by comparing the residuals of BVIJHK period-luminosity relation with residual of period-wesheit relation. In his paper, Madore had used V - I based wesenheit function to determine the errors and ultimately tighten the multiband PL relations. In this thesis, first, I applied the same method on B - V, V - K and J - K based wesenheit functions, and compared the deviation in resulting distance-reddening error-pair for individual star, for each color index case. Secondly, I modified the methodology from generic wesenheit function to composite wesenheit function and repeated the exercise to derive the error-pairs for individual Cepheid for each color indicies. It lead to some crucial insights about wesenheit function and its dependency on the reddening ratio and color index. Finally, the calibrated Leavitt Law cross-validated with an additional dataset of 18 Galactic cluster Cepheids - more reliable distance measured by averaging parallax of the cluster members hosting the Cepheids.

This part of the thesis ends with a discussion on the results.

1.3.3 Result Implications

LMC & SMC Distance

To test the effectiveness, LMC and SMC distances have been derived for 24 versions of calibrated Leavitt Law, i.e. 6 photometric bands with 4 colors of wesenheit functions. With such multiple possibilities, a distance matrix can be made highlighting effectiveness of particular color index used

in calibration, with respect to the rest.

In astronomy, distance is not just a measurement - it's the foundation upon which our understanding of the universe is built. From determining the true luminosity of celestial bodies to constraining the age, scale, and rate of expansion of the cosmos, accurate distance measurements are indispensable. The physical interpretation of almost every astronomical observation - be it the brightness of a star, the motion of a galaxy, or the composition of the universe - depends critically on knowing how far away the object lies. Throughout this section, we will see how the knowledge of distance informs our understanding of cosmic composition, the expansion rate, or the evolution of the Universe.

Composition of Universe

Given the vastness of the universe, it is natural to wonder what it is made of. A simplified answer might be that it consists of energy and spacetime. However, energy manifests in several distinct forms undergoing different physical processes and laws. It can be heat, mass, radiation or of any other form.

In cosmological terms, ordinary matter, referred to as *baryonic matter*, comprises electrons, protons, and neutrons, and constitutes only about 5% of the total energy content of the universe. This baryonic matter forms the stars, galaxies, and large-scale structures we observe today. In addition to baryonic matter, dark matter represents another critical component of the cosmos. Dark matter is hypothesized to possess fundamentally distinct properties from ordinary matter, as it neither emits nor absorbs electromagnetic radiation, rendering it invisible. Its presence is inferred solely through its gravitational effects. Dark matter accounts for approximately 27% of the universe's total energy content. Strong observational evidence for dark matter emerges from phenomena such as gravitational lensing, the anomalous rotation curves of galaxies, and the fine-scale anisotropies in the Cosmic Microwave Background (CMB). These observations, however, rely heavily on accurate distance measurements. For instance, the interpretation of gravitational lensing patterns and galaxy rotation curves depends critically on the precise determination of the distances to the lensed or orbiting objects. Despite its discernible gravitational influence, the precise nature and composition of dark matter remain unresolved, rendering it one of the most significant unsolved problems in contemporary astrophysics.

On cosmological scales, observational data further indicates that the universe is expanding at an

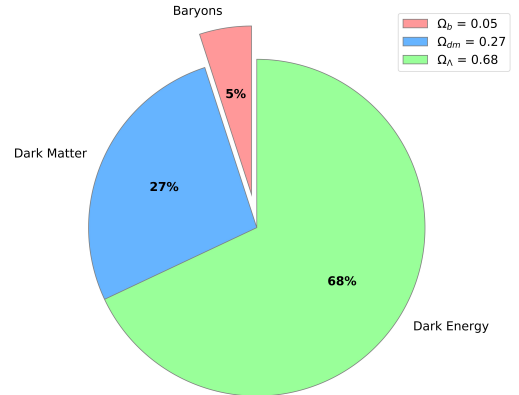


Figure 1.8: The fractional composition of the Universe consists of dark energy (68 %), dark matter (27 %), and baryonic matter (5 %) is depicted, with the contributions from radiation and other relativistic particles neglected. Strong observational

accelerating rate, a phenomenon attributed to a hypothetical form of energy known as dark energy. Like dark matter, the exact nature of dark energy is still unknown, but it is postulated to comprise approximately 68% of the total energy density of the universe. In stark contrast, other components, such as radiation, neutrinos, and various exotic non-baryonic particles, collectively account for less than 1%. The study of the distribution and evolution of these components remains a vibrant and evolving field of inquiry in modern cosmology.

The determination of the relative proportions of these matter and energy components hinges on precise distance measurements across cosmic scales, as these distances are pivotal in estimating both the observed brightness and redshift of distant objects—crucial factors in reconstructing the universe’s overall composition.

Hubble Constant and Cosmic Distance Ladder

One of the most pressing issues in modern cosmology is the growing discrepancy in the measured value of the Hubble constant (H_0)—the rate of expansion of the universe. Early-universe measurements, primarily derived from observations of the Cosmic Microwave Background (CMB) using the Planck satellite and interpreted within the Λ CDM cosmological model, yield a value for H_0 that significantly differs from those obtained via direct measurements in the local universe (Akrami et al., 2020; Freedman, 2021). This tension, now known as the *Hubble tension*, challenges our understanding of cosmology and may point to new physics or systematic errors yet to be uncovered.

Late-universe estimates of H_0 are derived by correlating redshifts with distances of astronomical objects. Because no single method spans the full range of cosmic distances, astronomers rely on a sequence of interconnected techniques known as the *cosmic distance ladder*. Each “rung” of the ladder is calibrated by more fundamental, closer-range methods to extend reliable distance measurements farther into the universe.

A key breakthrough in refining the distance ladder came from Adam Riess and collaborators, who studied Type Ia supernovae (SNIa) in distant galaxies. These explosive events, originating from white dwarf mergers, follow a predictable relation between their intrinsic brightness and the width of their light curves. By calibrating SNIa with Cepheid variable stars via the Leavitt Law, Riess extended high-precision distance measurements from the local 30 Mpc range ($\sim 10^8$ ly, Cepheid-based) to beyond 1000 Mpc ($\sim 10^{10}$ ly) using SNIa as *standard candles*.

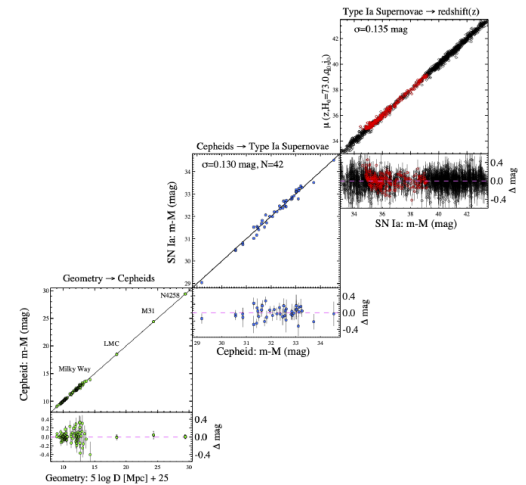


Figure 1.9: An instance of Cosmic Distance Ladder calibrating Leavitt Law with parallax, SNIa with Leavitt Law and Hubble Law with SNIa based distances. (Riess et al., 2022)

dles—objects with known intrinsic luminosity (Riess and Filippenko, 1998).

Figure 1.9 illustrates the cosmic distance ladder, starting from geometric parallax for nearby stars, advancing through Cepheid variables, and culminating in SNIa-based distances for high-redshift galaxies. Using this refined framework and fitting distances to the Hubble law derived:

$$H_0 = 73.30 \pm 1.04 \text{ km s}^{-1}\text{Mpc}^{-1}$$

a result in 5σ tension with the Planck-inferred value under Λ CDM assumptions (Riess et al., 2022). Resolving this discrepancy remains a top priority in cosmology, potentially revealing insights into dark energy, new particles, or modifications to the standard model of the universe.

Λ CDM Cosmological Model

By integrating observational data with the initial conditions established by Big Bang cosmology, scientists have formulated a standard cosmological model known as the Λ CDM (Lambda Cold Dark Matter) model. This model is defined by key parameters, including the densities of dark energy, dark matter, and baryonic matter; the Hubble constant (H_0); the scalar spectral index (which describes primordial density fluctuations); and the curvature parameter (which determines the geometry of the universe). Many of these parameters are tightly constrained using cosmic microwave background (CMB) measurements and are supported by various independent astronomical observations.

Accurate knowledge of cosmic distances is essential for estimating these parameters. The expansion rate, for instance, is inferred from the relationship between redshift and distance (the Hubble Law), while the discovery of the universe's acceleration was made possible by analyzing the luminosity of distant Type Ia supernovae.

Despite their differences in physical nature, the topics above share a common goal: the determination of distances to astronomical objects in order to accurately derive other physical parameters, such as size, mass, and age. Building on this idea, the primary focus of my master's thesis is to explore distance determination methodologies, with a particular emphasis on the Leavitt Law, and to improve its accuracy by identifying and addressing sources of systematic errors. With final remarks on results implication, the last chapter concludes this thesis.

Part I

Parameters of Leavitt Law

2 Observables - Luminosity, Reddening, Distance

2.1 Why does a star shine?

The Sun, a luminous and intensely hot star, derives its fundamental properties from the enormous gravitational forces acting within its structure. Possessing a mass approximately 333,000 times that of Earth, the Sun's vast mass is confined within a relatively compact volume, resulting in a continuous gravitational contraction toward its core. This inward collapse generates extremely high pressures and densities, particularly in the central regions. Consequently, core temperatures rise to several million Kelvin, establishing the conditions necessary for nuclear fusion to occur. Within this high-energy environment, surpassing the Coulomb barrier protons collide and fuse to form heavier atomic nuclei, predominantly helium.

At the core of the Sun, approximately 700 million metric tons of hydrogen are converted into helium each second through fusion processes, liberating a tremendous amount of energy. A substantial fraction of this energy is carried away by neutrinos, with a minor portion possibly emitted as gravitational waves. The remainder propagates outward as electromagnetic radiation, manifesting primarily as heat and visible light. This radiant energy escapes the solar surface and travels through space as sunlight, a fraction of which reaches Earth. Upon entering Earth's atmosphere, solar radiation interacts with atmospheric molecules, undergoing scattering that redistributes the light. The portion of the electromagnetic spectrum that penetrates the atmosphere - referred to as the optical band - corresponds to the visible range and is perceived as the bright solar illumination observed from Earth.

The total energy emitted by the Sun across all wavelengths per unit time is defined as its luminosity.

As this radiation traverses the Earth's atmosphere, part of it is absorbed or scattered, a process collectively termed atmospheric extinction. This mechanism modulates both the intensity and spectral distribution of solar radiation at the Earth's surface. A similar attenuation of starlight occurs in interstellar space, known as *interstellar extinction*, wherein light is absorbed or scattered by interstellar dust and gas. This process affects the transmission of radiation between stellar sources rather than through a planetary atmosphere.

A notable consequence of extinction is the wavelength-dependent nature of absorption and scattering, a phenomenon known as *reddening*. Because shorter wavelengths (i.e., blue light) are more efficiently scattered than longer wavelengths (i.e., red light), light passing through such media often exhibits a shift toward redder colors. This reddening effect serves as a crucial diagnostic tool in astrophysics, enabling the characterization of the intervening interstellar medium and enhancing our understanding of the distribution and composition of cosmic dust and gas.

2.2 Light: Color and Luminosity

Light is a form of electromagnetic (EM) radiation that travels through space at a constant speed of 299,792,458 meters per second in a vacuum. The human visual system is sensitive to a narrow portion of this spectrum, known as the optical band, which ranges from approximately 350 to 700 nanometers wavelength. This segment represents only a small fraction of the full electromagnetic spectrum, which spans from high-energy gamma rays to low-energy radio waves.

The electromagnetic spectrum also describes the distribution of thermal radiation emitted by objects at various temperatures. When matter is heated, it emits energy in the form of electromagnetic radiation. As the temperature increases, the peak of this emission shifts toward shorter wavelengths and higher frequencies, corresponding to a greater energy output. This fundamental relationship between temperature and spectral energy distribution (SED) is described by Planck's law (Planck, 1900), which provides the theoretical foundation for the modern understanding of blackbody radiation and underpins much of contemporary astrophysics.

According to Plank law, a perfect black body absorbs all the incident radiation and emits radiation across the entire electromagnetic spectrum. His formulation of spectral energy distribution as a function of wavelength is given as:

$$B_\lambda(T) = \frac{8\pi hc}{\lambda^5(e^{\frac{hc}{\lambda kT}} - 1)} \quad (2.1)$$

where B_λ is radiant energy at given wavelength in $[W.m^{-2}.sr^{-1}.m^{-1}]$ unit, λ is wavelength, h is Planck's constant, k is Boltzmann constant, c is speed of light and T is the temperature of the object. Integrating it for all the wavelength yields the total energy output of the blackbody at given temperature.

To estimate radiation flux emitted towards the observer, integrating $B_\lambda(T)$ over the hemisphere

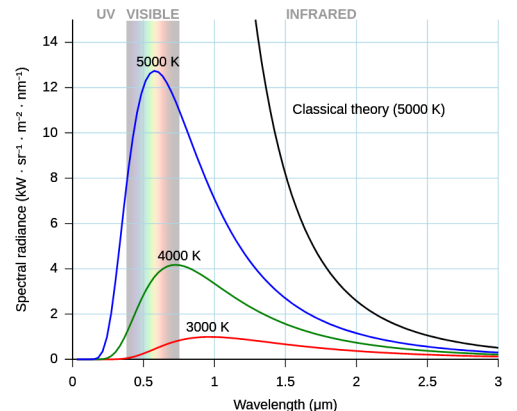


Figure 2.1: *Black body radiation curves based on Planck's Law for various temperatures. The maxima of the curves shift according to Wien's displacement law. Source: Wikipedia commons*

above the emitting surface:

$$F_\lambda(T) = \int B_\lambda(T) \cos\theta d\omega = \pi B_\lambda(T) \quad (2.2)$$

Now, consider a star of radius R that emits a spectral radiation flux F_λ at temperature T . At a distance d from the star, the flux measured by a detector is governed by the inverse-square law, which states that the observed flux decreases with the square of the distance from the source. Accordingly, the observed flux f_λ at distance d is given by:

$$f_\lambda = \frac{R^2}{d} F_\lambda \quad (2.3)$$

If the sensitivity of detector given by sensitivity function, E_λ , the total radiation flux received by the detector would be

$$s = \int_0^\infty f_\lambda E_\lambda d\lambda \quad (2.4)$$

The amount of flux received by a detector measured as photon count per wavelength range, called as *band*, which further converted into more convenient unit of measurement called as *magnitude*. It is the standard unit of measurement of light in photometry.

2.2.1 Magnitude Scale

Ancient Greek astronomer, Hipparchus (c. 190 – c. 120 BCE), had made a star catalogue by defining a scale of brightness for stars in the units of magnitude (mag), where '1 mag' refers to the brightest and 6 mag is the dimmest star in the sky, for unaided eye. The definition of magnitude scale revisited by V.Pogson in 1850 and calibrated by J.F. Zöllner in 1861 by using visual photometer. They made a comparison between an artificial star and a real star using two Nicol prisms to redefine a precise magnitude scale.

According to Pogson's definition, difference between 'apparent magnitudes' of two stars is proportional to the logarithmic of their radiation flux ratio (s_1/s_2). i.e.

$$m_1 - m_2 = 2.5 \log(s_1/s_2) \quad (2.5)$$

It follows as if the magnitude of two stars differ by 5, that means one star appears 100 times brighter than the other star. For instance, it is measured that α Lyr (Vega) has visual magnitude of 0.14 mag and α Cyg (Deneb) has 1.33 magnitude which is fainter than α Lyr. Sun, Moon, Venus, Mars, Jupiter and three stars - Sirius, Canopus and α Centauri are the only celestial objects having

negative apparent magnitude, count among the brightest objects in the night sky.

2.2.2 Color Index ($m_1 - m_2$)

The visible band of light is a small window of electromagnetic spectrum corresponds to the wavelength ranging from 300 nm (Blue) to 700nm (Red). The difference in the photon intensity at different wavelength translated as different color index. If one observes the night sky carefully, it would be clear that stars come in different colors, and their magnitude differs on observing with different color bands. For instance, if one observes the sky in red band, Betelgeuse would appear brighter than Sirius, even if Sirius is the brightest star. It is because Sirius emits its most of the radiation in blue band, while betelgeuse radiates in red band. It is due to their photosphere's temperature differences.

To determine the precise stellar colors and magnitudes, W.W. Morgan and H. L. Johnson developed UBV system of color bands with effective wavelength for ultraviolet $_{\lambda} : 365$ nm , blue $_{\lambda} : 440$ nm, visual $_{\lambda} : 548$ nm) (Johnson and Morgan, 1953). Further extension of the UBV system into the red and infrared passband was done by adding following filters in [μm].

<i>Bands</i>	<i>R</i>	<i>I</i>	<i>J</i>	<i>H</i>	<i>K</i>	<i>L</i>	<i>M</i>	<i>N</i>	<i>Q</i>
λ_{eff}	0.7	0.9	1.25	1.63	2.2	3.6	5.0	10.6	21

Temperature (T_{eff})

While studying stellar spectra, K. Schwarzschild recognised that the color incides measures the energy distribution, thus it could be used to estimate the temperature of photosphere of the star.

On fitting energy distribution with Plank radiation law, in Wien's approximation ($c_2/(\lambda T) \gg 1$), the radiation flux results

$$F_{\lambda} \propto \exp(-c_2/(\lambda T_c)) \quad (2.6)$$

For the sake of simplicity, let the sensitivity function of the photo-detector be at its maxima, then the relation in between color index, B - V , and the effective temperature of the star would be.

$$B - V = \frac{2.5c_2 \log e}{T_C} \left(\frac{1}{\lambda_B} - \frac{1}{\lambda_V} \right) + const. \quad (2.7)$$

with radiation constant $c_2 = 0.014mK$, $\lambda_B = 440nm$ and $\lambda_V = 548nm$,

$$B - V = \frac{0.7 * 10^4}{T_c} + const. \quad (2.8)$$

The above equation suggests that the color indices (B-V) corresponds to temperature of the star.

Referring α Lyr (Vega - A0V type star) as a standard star, the magnitude scale, in U, V and B bands, defined in such a way that :

$$U - B = B - V = 0 \implies C_{UB} = C_{BV} = 0 \quad (2.9)$$

For convenience, the notation for color $U - B$ is adopted as C_{UB} . Color index C_{BV} less than 0.5 indicates blue and more than 1.5 indicates red.

2.2.3 Absolute Magnitude (M)

When a luminous object is observed from different distances, it appears to have varying brightness because flux decreases with increasing distance. So, how can we compare the intrinsic brightness of two remote stars? To enable standardized comparisons, astronomers adopt a reference distance of 10 parsecs (pc). The radiant flux of a star measured at this distance defines its *absolute magnitude*, denoted as M_λ . The subscript λ indicates the specific photometric band (filter) used in the observation, as brightness varies across different bands.

Given this framework, if m_λ represents the apparent magnitude of a star observed at a distance d (in parsecs), and M_λ is its absolute magnitude, the relationship between them is given by the following formula:

$$M_\lambda = m_\lambda - 2.5 \log \left(\frac{d[pc]}{10} \right)^2$$

$$M_\lambda = m_\lambda - 5 \log d[pc] + 5 \quad (2.10)$$

The above is a simple relation which relates the observable luminosity with the distance of any stellar object.

Note 2.2.1: True Absolute Magnitude

The above relation must be corrected for the effect of interstellar extinction, A_λ , to obtain the correct '*photometric*' distance.

$$M_\lambda^0 = m_\lambda - A_\lambda - 5 \log d[pc] + 5 \quad (2.11)$$

2.3 Distance

The introductory chapter makes it clear that the standard units of length used in everyday life are inadequate for astronomical measurements. To address this, astronomers have developed a distinct set of units for measuring astronomical distances. However, different units are used depending on the spatial scale. For example, within the solar system, the astronomical unit (AU) is sufficient, while on the scale of the Milky Way, the light-year is more appropriate. For even larger distances, such as those in extragalactic realm, units like the parsec or megaparsec are commonly used. The relationships between these units are summarized in Table 2.1.

Table 2.1: Conversion of Astronomical Distance Units

	Kilometer	Astronomical Unit	Light Year	Parsec
Kilometer	1			
Astronomical Unit	149597870.700	1		
Light Year	9460730472580.8	63241.077	1	
Parsec	30856775814913673	206264.806247096	3.261563777	1

2.3.1 Parallax: Measuring Astronomical Distances Using Geometry

Parallax is a geometrical method that utilizes trigonometric principles to measure the distance to an object by observing its apparent shift relative to a fixed background, caused by the movement of the observer. While measuring distances between nearby objects on Earth is straightforward using tools like rulers or laser rangefinders, this becomes impractical when dealing with vast astronomical distances. Hence, astronomers rely on methods such as parallax, Leavitt Law, etc.

The choice of method for measuring astronomical distances depends on both the scale of the measurement and the characteristics of the celestial object in question. Since no single technique is effective across all distance ranges in the universe, astronomers must understand the physics of various astrophysical phenomena in order to select the most appropriate method for a given situation. Accurate distance measurement is foundational in astronomy, as it affects our understanding of everything from stellar properties to the large-scale structure of the cosmos.

One of the fundamental tools used in determining distances is trigonometry. In a right-angled triangle, if one side and an angle (other than the right angle) are known, the other sides can be calculated using trigonometric ratios. There are six basic trigonometric functions: sine (sin), cosine (cos), and tangent (tan), along with their respective reciprocals: cosecant (csc), secant (sec), and cotangent (cot). These ratios depend solely on the angle and not on the actual size of the triangle, making them highly useful in astronomical applications where distances are vast and direct measurement is impractical.

In the context of stellar parallax, a conceptual triangle is formed between the Earth, the Sun, and a distant star. The baseline of this triangle is the distance between the Earth and the Sun, known as 1 Astronomical Unit (AU). As Earth moves in its orbit over the course of six months, nearby stars appear to shift slightly against the backdrop of more distant stars. This apparent angular shift is called the parallax angle. Because the triangle formed is extremely elongated, the parallax angle is very small, typically measured in arcseconds.

To calculate the distance to a star using the parallax method, astronomers apply the tangent trigonometric ratio, which in this context is:

$$\tan p = \frac{1AU}{d} \quad (2.12)$$

For very small angles (as in astronomical observations), $\tan p$ is approximately equal to p when measured in radians. Therefore, the distance can be simplified to:

$$d = \lim_{p \rightarrow 0} \frac{1AU}{\tan p} = \frac{1AU}{p} \quad (2.13)$$

To standardize distance measurements, astronomers use the parsec as a unit of length.

1 parsec (pc) is defined as the distance at which 1 AU subtends an angle of 1 arcsecond (1/3600 of a degree).

The Gaia satellite, launched by the European Space Agency in 2014, has revolutionized our understanding of the Milky Way by measuring the parallax and proper motion of billions of celestial objects. Among the vast number of objects observed, several notable types of variable stars, including Cepheid variables and RR Lyrae stars, were also studied. In this thesis, the parallax-driven distances provided by Gaia will be used to calibrate the period-luminosity relation.

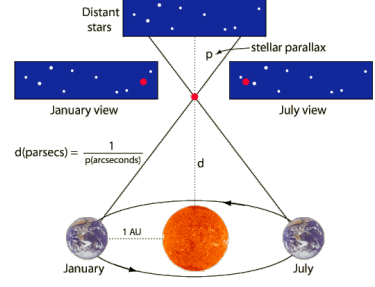


Figure 2.2: As Earth orbits the Sun, nearby stars appear to shift against distant background stars—this shift, called parallax, is used to measure their distance using trigonometric ratio.
Source: hyperphysics.phy-astr.gsu.edu

2.3.2 Distance Modulus (μ)

A useful parameter for denoting distance in astronomy is the distance modulus, μ , which provides a logarithmic transformation of the distance to an object, using 10 parsecs as the reference distance. The distance modulus can also be expressed as the difference between the apparent magnitude and the absolute magnitude of an object. Mathematically, it is formulated as:

$$\mu = m - M = 5 \log_{10} \left[\frac{d}{10pc} \right]$$

2.4 Interstellar Reddening

In photometric observations, the electromagnetic flux of starlight is quantified by counting the incoming photons within a specific wavelength range of the spectrum. Intervening gas in interstellar space absorbs most of the high-energy photons (X-rays and extreme ultraviolet, EUV) and scatters much of the light in the B and V bands. Radiation with wavelengths longer than the size of dust particles can pass through the interstellar medium largely unaffected, making the sky nearly transparent to infrared, microwave, and radio waves. The diminishing of short-wavelength luminosity makes the source appear redder than its intrinsic color, giving rise to the effect known as reddening.

This phenomenon can be illustrated by comparing the observed SED of stellar light to the theoretical SED predicted by Planck's Law, as shown in Figure 2.4.

Let B and V be the apparent luminosities of a star as received by the observer, while B_0 and V_0 represent the intrinsic (unextincted) luminosities. Then, the effect of extinction can be formulated as follows:

$$A_B = B - B_0 \quad (2.14)$$

$$A_V = V - V_0 \quad (2.15)$$

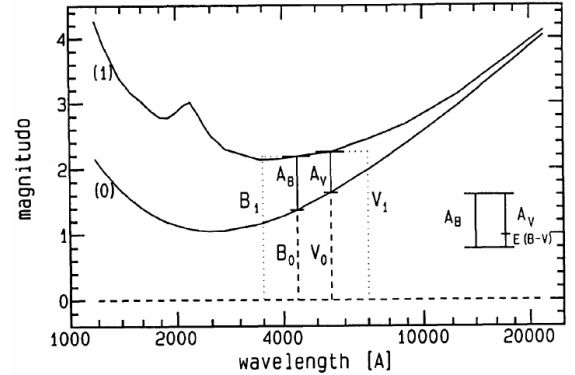


Figure 2.3: Comparision between emitted (0) and observed (1) SEDs. For given band, deviation between the curves represents interstellar extinction (here, A_B and A_V). On the right side, the relative difference between extinction of two bands depicting the definition of interstellar reddening $E(B - V)$. (Krelowski and Papa, 1993)

The difference between the two defines the *color excess* - that is, the deviation of a star's apparent color from its intrinsic color.

$$E(B - V) = A_B - A_V = (B - V) - (B - V)_0 \quad (2.16)$$

Color excess is more widely used than extinction to describe the effect of the ISM on starlight, as it can be measured photometrically even when the intrinsic brightness of the star is unknown.

2.4.1 Reddening Ratio

The ratio of total-to-selective absorption, R_λ summarizes the effect of extinction and reddening on the intensity of light along the line-of-sight. It is formulated as:

$$R_{\lambda}^{BV} = \frac{A_{\lambda}}{E(B-V)} \quad (2.17)$$

For Milky Way, the reddening ratio in V-band, R_V , is evaluated about 3.23 (Sandage et al., 2004), whereas in B-band it set to be as $R_B = R_V + 1$

Rearranging the above relation and writting it as:

$$A_{\lambda} = R_{\lambda} E_{BV} = R_{\lambda} (A_B - A_V) \quad (2.18)$$

The above equation is used for transforming measured color excess into extinction for any band, provided R_{λ} is priorily known. Rearranging it further, for V-band, the equation takes the form:

$$\frac{A_B}{A_V} = 1 + \frac{1}{R_V} \quad (2.19)$$

Cardelli et al. (1989) generalised the extinction law in this form for all the bands with V-band as reference as discussed in the following section.

An another important aspect of the reddening ratio is to convert color excess from one pair of bands, say E_{BV} to another, E_{12} . It can be done as follows:

$$E_{12} = (R_1^{BV} - R_2^{BV}) E_{BV}$$

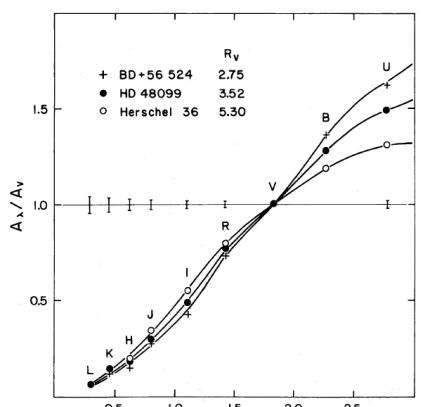
This leads the transformation law for reddening ratio R_{λ} :

$$R_{\lambda}^{12} = \frac{R_{\lambda}^{BV}}{R_1^{BV} - R_2^{BV}} \quad (2.20)$$

The values of R_{λ}^{BV} are calculated by Fouqué et al. (2007) and given in Table 2.2.

2.4.2 Interstellar Extinction Law

Observations of the spectral energy distribution (SED) of stellar light by Whiteoak (1966) demonstrated the diminishing effect of interstellar extinction at longer wavelengths. This finding led to the formulation of an extinction law - an inverse relation between extinction and the wavelength of stellar light.



In its simplest form, the extinction law formulated as ([Cardelli et al., 1989](#)):

$$\frac{A(\lambda)}{A(V)} = a(\lambda^{-1}) + \frac{b(\lambda^{-1})}{R_V} \quad (2.21)$$

Here $a(\lambda^{-1})$ and $b(\lambda^{-1})$ are determined empirically for different spectral ranges. Since, historically, observational data in the V-band were available for most stars, extinction in the V-band has been used as a reference. The Figure 2.4 depicts that a variation in R_V leads to changes in extinction law, where short wavelength have significantly affected as compared to longer wavelengths. Using the averaged value over all the directions in the Milky Way for $R_V = 3.23$ and the formulation (2.21), [Fouqué et al. \(2007\)](#) evaluated the extinction law for BVRIJHK bands as given in the Table 2.2

Table 2.2: Extinction Law and corresponding reddening ratio adopted from Table 4 of [Fouqué et al. \(2007\)](#)

Band filters	Effective Wavelength λ (μm)	Extinction Law $\frac{A(\lambda)}{A(V)} = a_\lambda + \frac{b_\lambda}{R_V}$	Reddening ratio $R_\lambda = \frac{A_\lambda}{A_V} \times R_V$
B	0.438	1.31	4.231
V	0.545	1	3.230
I	0.798	0.608	1.963
J	1.235	0.292	0.943
H	1.662	0.181	0.584
K	2.159	0.119	0.384

2.4.3 Wesenheit Magnitude

To account for the effects of reddening, [Madore \(1982\)](#) introduced a method based on a pseudo-magnitude derived from the reddening ratio, known as the Wesenheit magnitude. By definition, this quantity is constructed to be free from the effects of reddening. Its mathematical formulation is derived as follows:

$$R_\lambda^{12} = A_\lambda/E_{12}$$

$$= \frac{m_\lambda - m_\lambda^0}{(m_1 - m_2) - (m_1 - m_2)_0}$$

On rearranging the terms,

$$m_\lambda - R_\lambda^{12}(m_1 - m_2) = m_\lambda^0 - R_\lambda^{12}(m_1 - m_2)_0 \quad (2.22)$$

$$W_\lambda^{12} = W_0 \quad (2.23)$$

It can be observed that, on the left-hand side, all terms except R are observables, while the right-hand side consists of absolute quantities. This implies that if R is known a priori with high precision, the Wesenheit magnitude will yield the same value for both reddened and unreddened sources, effectively making it a reddening-free parameter.

Note 2.4.1: Equivalent Wesenheit Magnitude

For wesenheit magnitude, the following relation holds true for any color index $(m_1 - m_2)$

$$W_1^{12} = W_2^{12} \quad (2.24)$$

A comparison of the definitions of the 'true' absolute magnitude and the Wesenheit magnitude in relation to the color index (B-V) reveals:

$$M_\lambda^0 = m_\lambda - R_\lambda^{BV} \times E(B - V) - \mu \quad (2.25)$$

$$W_\lambda^{BV} = m_\lambda - R_\lambda^{BV} \times (B - V) - \mu \quad (2.26)$$

It can be observed that absolute magnitude depends on four types of measurements: photometric magnitude, distance, reddening ratio and color excess. In contrast, Wesenheit magnitude requires only three types of measurements and does not depend on color excess. Let's examine how these magnitudes vary with errors in measurement. Assuming that the *apparent luminosities are precisely measured ($\delta m_\lambda = 0$), the adopted extinction law is accurate ($\delta R = 0$), implies the errors contribution divided among the distance modulus ($\delta\mu$) and color excess (δE_{BV}) measurements* in the case of an individual Cepheid. Error in above equations leads to:

$$\delta M_\lambda = -(R_\lambda^{BV} * \delta E(B - V) + \delta\mu) \quad (2.27)$$

$$\delta W_{\lambda}^{BV} = -\delta \mu \quad (2.28)$$

This pair of equations indicates that both the Wesenheit magnitude and the absolute magnitude are sensitive to distance errors. However, unlike the absolute magnitude, the Wesenheit magnitude remains unaffected by errors in reddening. This characteristic of the Wesenheit magnitude is particularly important, as it helps to decouple the errors contributions of distance and reddening for individual Cepheids.

Application of these equations in the Leavitt Law calibration will be discussed in the *Part II* of this thesis.

3 Pulsating Star - Classical Cepheid

3.1 Are all stars the same?

Seeing the night sky, one can easily spot that stars come in different colors and luminosities, making it easy to infer that not all stars are the same. But what makes them appear different? With the advent of quantum mechanics and spectroscopic observation, this question was answered by suggesting the physical processes occurring inside the star, along with its changing chemical potential over the different evolutionary phases. It has been observed that some stars can be thousands of times larger than others—such as red giants and supergiants—while others undergo radial oscillations periodically, like RR Lyrae, Cepheids, and Mira variables. Some stars may form diffuse gaseous systems, such as protostars and planetary nebulae, while others could be the remnants of dead stars, like white dwarfs or neutron stars. These examples represent different phases in the life cycle of a single star. This chapter delves into these evolutionary stages, examining how astronomers classify stars, discussing their underlying physics, while focusing particularly on Cepheid variables.

3.1.1 Discovery of Variable stars

The year 1784 is significant in astronomy, as it was when John Goodricke observed the period variation of a star - Delta Cephei - challenging the centuries-old belief that the sky is static, with all stars being fixed and unchanging. Motivated by such a remarkable discovery, the hunt for more variable stars began. Inheriting the name from the first one, variable stars of a similar class were classified as Cepheid variables. Until the twentieth century, it was unclear to astronomers why Cepheids vary in luminosity. Some suggested a pair of eclipsing binaries, others proposed interior effects due to stellar magnetic fields, while some supported the idea of radial pulsation in the star's envelope. A notable contribution from Arthur Eddington played a central role in the development of the pulsation theory. Mimicking the physics of a reversible heat engine and conceptualized through the kappa mechanism (derived from a valve periodically blocking and releasing heat), Eddington formulated the pulsation theory of Cepheid variables.

Further developments by Chandrasekhar in the hydrodynamic and magnetohydrodynamic stability provided a foundational approach for modelling stellar pulsation for different masses in various

phases. By modeling chemical composition and drawing inspiration from Eddington's valve mechanism for stellar pulsations, Zhevakin, in 1953, proposed that the cyclical ionization of helium drives the radial oscillations observed in Cepheid variables (?). He modeled a spherical shell consisting of an 85%–15% hydrogen–helium mixture (by number of atoms), where helium transitions between the transparent HeI and opaque HeIII states. These ionization transitions modulate the opacity of the stellar envelope, leading to variations in surface brightness and pulsation behavior in Cepheids.

Building upon Chandrasekhar's framework, Cox work on stability of Cepheid variable utilising hydrodynamic theory with thermal condition to yield the equation of state of such radially oscillating system. His contribution through non-adiabatic pulsation theory explained κ - mechanism - how ionized Helium layers changes opacity causing instability region in Hertzsprung-Russell diagram called instability strip.

3.2 Color-Magnitude Diagram

Over its entire lifecycle, star varies its brightness and luminosity according to its phase of life. Ernheprung was the first who plotted the brightness of the star cluster with respect to its color, and understand the evolutionary trend hidden in the plot. Soon after, Rusell also came to similar conclusion independently. In their honor, color-magnitude diagram also termed as HR diagram.

3.2.1 Spectral Classification

Everything in the universe has a beginning and its end, stars are not the exception. In the course of millions to billions of years, stars take birth in the vicinity of gas clouds, called *Nebula*, due to the gravitational collapse of the clouds. Due to high temperature and pressure at the core, they fuse primordial particles to heavier elements and release immense amount of heat and radiation - part of which we perceive as visible light. The evolution of a star primarily depends on its initial mass. Massive stars impose high gravitational pressure, raise the higher temperature at the core consequently fusing elements faster. This makes massive stars live shorter as compared to low-mass stars. In their evolutionary process, stars pass through several phases depending upon their internal processes, driven by their mass. The consecutive evolutionary stages of stars with different initial masses are depicted in the Figure 3.1.

3.2.2 Stellar Evolution

The stars we see in the night sky are made up of diffused interstellar gases, primarily Hydrogen and Helium. At some point in the history of stellar evolution, the diffused gases became gravitationally bounded and formed molecular clouds in the vicinity of spacetime. As the matter accumulates in a region, the curvature of spacetime arises which accelerates the gravitational collapse of matter.

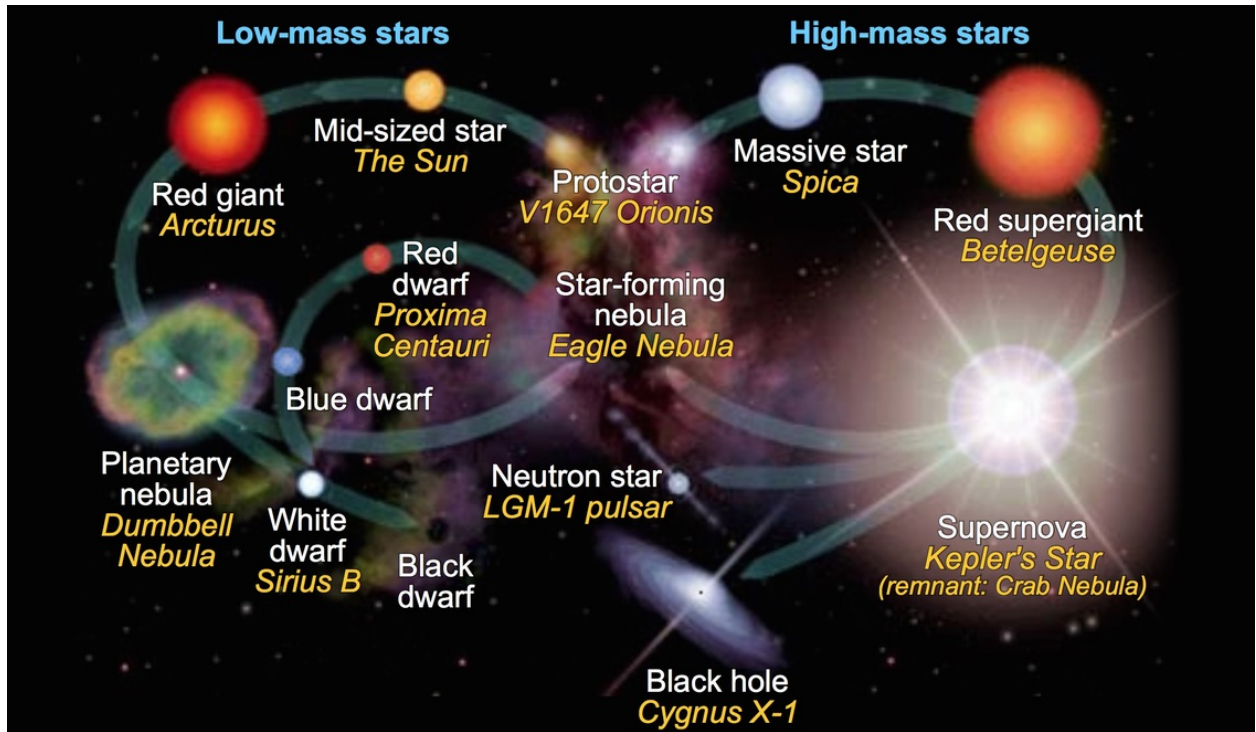
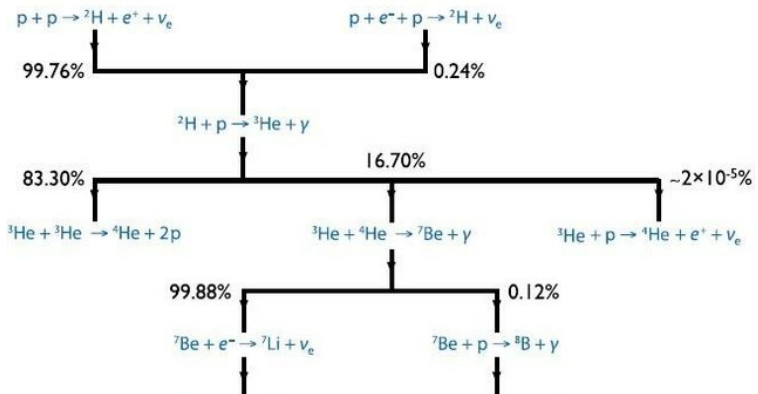


Figure 3.1: Evolutionary cycle for low and high mass star. Low mass stars, like Sun, become a Red Giant when Hydrogen supply to the core stops and fusion takes place in the shell around the core. Afterwards they become a Planetary nebula with a bright core at the center and end their life as a White Dwarf, slowly get faded turning into brown dwarf. Massive stars evolve to Red Supergiant and end their life as Supernova leaving behind either a Neutron star or Black Hole. [cmglee/NASA Goddard Space Flight Center]

Due to relatively higher pressure than the surrounding, a temperature gradient towards the core of the gaseous cloud begin to form. With increasing density the temperature of the core rises steadily. Around the region of maximum curvature, the first hydrostatic core forms, with a temperature range of 60-100K, which halts the gravitational collapse. According to virial theorem, with the more mass the temperature continues to rise and the molecular Hydrogen starts to dissociate once the temperature reaches 2000K. The process continues until the outward pressure balances the gravitational collapse to attain the state of hydrostatic equilibrium. At this stage, *Hary-Halo object* forms at the core, surrounded by an accretion disc of matter which follows the *tendex line* - trajectory of matter falling into the central core.

Formation of Star

The primary condition for nuclear fusion is to have physical contact between two nuclei of atoms, but the nuclei repel each other due to the positive charge of the proton inside them. This repulsive force does not allow nuclear fusion to happen in normal conditions. The threshold en-

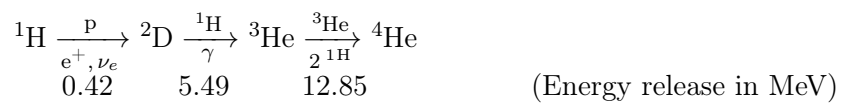


ergy requires to bring two like charged particles in contact is called the Coulomb barrier of the system. Hence, to initiate a nuclear fusion process, the repulsive force of nuclei needs to be overcome which is possible by achieving very high kinetic energy due to extreme temperature and high pressure. Such conditions can easily be fulfilled at the core of the stars. The moment when nuclear fusion takes place at the core of protostar, 4 Hydrogen fuses to form one Helium atom, that marks the birth of a star and the object called *main sequence* star.

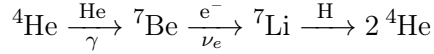
It is assumed that primordial gases would be made up of the simplest element possible, like Hydrogen because the existence of heavier elements than Hydrogen would require processes like nuclear fusion taken place priory. The first basic nuclear reaction, the formation of Deuterium (nucleus containing one proton and one neutron), requires a temperature of 10 - 18 million Kelvin. In this scenario, two protoniums (hydrogen ions) collide with each other at a very high velocity, surpassing the Coulomb barrier and entering to field of strong nuclear force at femto scale. Consequently, one of the protons emits its positive charge in the form of a positron with a neutrino particle, converting into a neutron. This process is called as β^- decay process. Both elementary particles, proton and neutron, stick together to form nucleus of Deuturium. Series of such nuclear reactions release an immense amount of energy radiating outwards. Radiation pressure counter balances the continous gravitation collapse of the matter, sustaining the spherical structure of the protostar for thousand to million years. The energy released from fusion reactions in stars calculated by Bethe and published under title - 'Energy production in stars' ([Bethe, 1939](#)). At the heart of these calculation, Einstein's famous equality $E = \Delta mc^2$ underliers. Here, c is the speed of light and Δm is the difference between the mass of reactants and products of the fusion reactions.

Proton-Proton Reactions: Efficient for $1 M_0$ star's core.

Branch I: 83.30% Helium production, at 10-18 MK



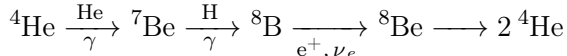
Branch II: 16.70 % Helium production, at 18-25 MK



1.59 0.861 17.35

(Energy release in MeV)

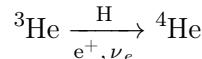
Branch III: 0.12% Helium production, above 25 MK



1.59 5.59 23.29

(Energy release in MeV)

Branch IV: 0.00002% Helium generation in Sun



19.795

(Energy release in MeV)

Main sequence star and Turn-off point

The color of the star gives a rough idea about the surface temperature as well as evolutionary phase of the star. Newly born stars are rich in Hydrogen and fuse it rigorously resulting very high surface temperature making it appear bluer. After millions of years, helium as byproduct accumulates at the core which blocks the supply of Hydrogen and reduces the rate of fusion due to which star cools down and turn yellowish. It is worth to say that, high mass stars exert high pressure at core and burn its fuel quickly as compare to low mass stars. Where lifespan of a high mass star ($8-10 M_\odot$) lies around 10-15 million years, for low mass star it can be 15-20 billion years. In its life journey, any star spends most of the time in Main Sequence phase.

For the case, when the initial mass of star remained under half of solar mass, after a few billion years, enough Helium get depleted at the core which blocks the hydrogen supply, ultimately reducing the rate of fusion reaction. Star gets cooler with time, finally become redder than a brown dwarf and its life as a black dwarf after trillions of year. Such star never leaves the main sequence but only changes its spectral type as it evolves. For star of one solar mass, when Helium core forms which reduces the rate of fusion reaction, the gravitation pull begins to contract the core and core's temperature increases again. With higher temperature, Hydrogen begins to fuse around the Helium core in a shell, making

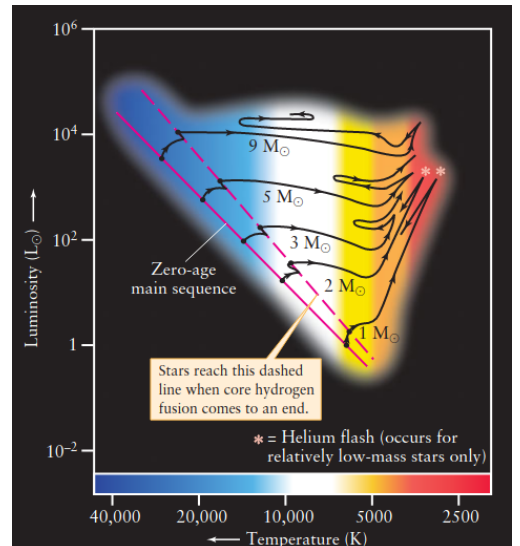


Figure 3.3: Isochrones of stars with different masses depicting their evolutionary tracks. Massive stars not Source: Universe (VIII edition) by Roger A. Freedman & William J. Kaufmann III

the star move away from the main sequence and marks the turn-off point in the HR diagram.

Red Giant Star and Helium Flash

Shell burning Hydrogen generates even more energy than core burning phases. Released energy pushes the envelope of matter outwards which expands the surface of the star enormously and it becomes a giant. With increased surface area and shell H-burning, luminosity of the star increases by the order 3 to 4, however, due to expansion, surface of the star cools down making it red in color. This physical characteristics gives it name - Red Giant. Further accumulation of Helium at the core due to H-shell burning continuous. Star having mass more than 3 solar mass, gradually star helium burning at the core, however stars with mass between 0.3 to 3 solar mass attain Helium fusion spontaneously, called as Helium Flash. For the latter case, central region of the core becomes incompressible but the rest of core still collapses causing further rise in temperature at center, but not sufficiently enough that helium could fuse, so the central core takes the form of degenerate matter to balance the gravitation collapse.

Around 300 million K, the degenerate matter spontaneously fuses into heavier elements, Carbon and Oxygen, by triple alpha process leaving behind a flash of high energy which rises the temperature exponentially high. Degenerate matter fuses rapidly rising the temperature even higher which accelerate the reaction rate. This thermal runaway reaction increases the energy production of the star to 100 billion times for a very short time, which is comparable to entire galaxy's energy output. Eventually thermal pressure becomes dominant and the core expands. This phase in HR diagram can be observed as the tip of the red gaint branch on the right-upper side for intermidiate mass (0.4 to 3 solar mass). Just after this state, star rearranges its structure rapidly and attain an equilibrium state with a lower luminosity but higher temperature than before. This spontaneous process shifts the star from red gaint branch to horizontal branch while leaving a discontinuity in between the two regions in HR diagram.¹

Horizontal branch and Variable stars

While evolving through horizontal branch, stars fuse Helium at the core and Hydrogen in a shell. Moving towards right side, star enters to the blue edge of instability strip of HR diagram where it experience a dynamic equilibrium between gravitational contraction of outer envelope and its thermal expansion due to energy generation from internal processes. This translated as a radial oscillatory motion of the surface, giving birth to a new category of stars called variable stars. In 1784, John Goodricke had discovered a variable star, δ Cephei, in Cepheus constellation and named the star as δ Cephei. After the discovery of a few more variable stars, the family of δ Cephei type stars called as Cepheid stars.

¹Kristen. B. W. McQuinn et al 2019 ApJ 880 63

Initially, it was assumed that the periodic variation of luminosity arising because the star is a member of eclipsing binary system. In 1917, Arthur Eddington rejected the prior theory and gave a clever explanation behind the radial pulsation of star by purposing a valve mechanism. His purposed mechanism known as Kappa mechanism as kappa stand for coefficient of absorption of stellar material. After excessive burn of hydrogen, helium becomes the next abundant element on the surface. Due to high temperature at the compressed state of Cepheid star, Helium releases its both electrons and get ionized He^{2+} . Opaque He^{2+} blocks the outcoming radiation making the star appear dimmer. The radiant energy develops a pressure and expands the star's surface. The expansion increases the surface area illuminating the star. Expansion also cools down the surface so the ionized Helium captures the free electrons and back to its ground state He. Neutral Helium is a transparent gas consequently, all the trapped radiation releases making the star even more luminous. As the radiation pressure decreases, the stellar surface begin to collapse again due to gravitational pull and shrinks down to original state. This brings the process to its initial state.

AGB Stars and Planetary Nebulae

In a time scale of 100 million years, star evolve through the instability strip and exits from red edge of the instability strip towards right in HR diagram. At this stage, Helium fusion process continues in a shell around the Carbon/Oxygen core making star luminous then Red Giant phase and even bigger in size, comparable to the orbit of the Earth. In HR diagram, it moves alongside the Red Giant branch which gives it name Asymptotic Giant Branch. After Helium shell runs out of fuel, outer layer of Hydrogen burning becomes the dominant source of energy and produces Helium. After 100 thousand years, Helium accumulates and ignites again spontaneously which expands the outer surface of the star even more. Expansion cools down the temperature which halts the Hydrogen shell burning. In the next hundreds of years, Helium burning stops and Hydrogen burning take place to produce more Helium. This cycle of energy production in shells along with Helium shell flash processes expel 50% to 70% of star's mass in the interstellar space, bringing AGB stars to its end as a planetary nebula. The radius of planetary nebula can reach upto 30 light years (nearest star to the Sun, Proxima Centauri is about 4.2 lightyears away).

White Dwarf and Super Novae

After fusing Helium and Hydrogen in shell, Carbon and Oxygen rich core forms at the center. By passing through AGB and then planetary nebula phase, star release its most of mass as stellar wind and the core remains as the remnant of dead star, countering the gravitational collapse by electron degeneracy pressure as there is not active nuclear fusion going on. Such an object is called White Dwarf. S. Chandrasekhar, in 1930s, developed a theory about such compact object and purposed that such object can not exceed its mass more than 1.44 times of solar mass. This number is known

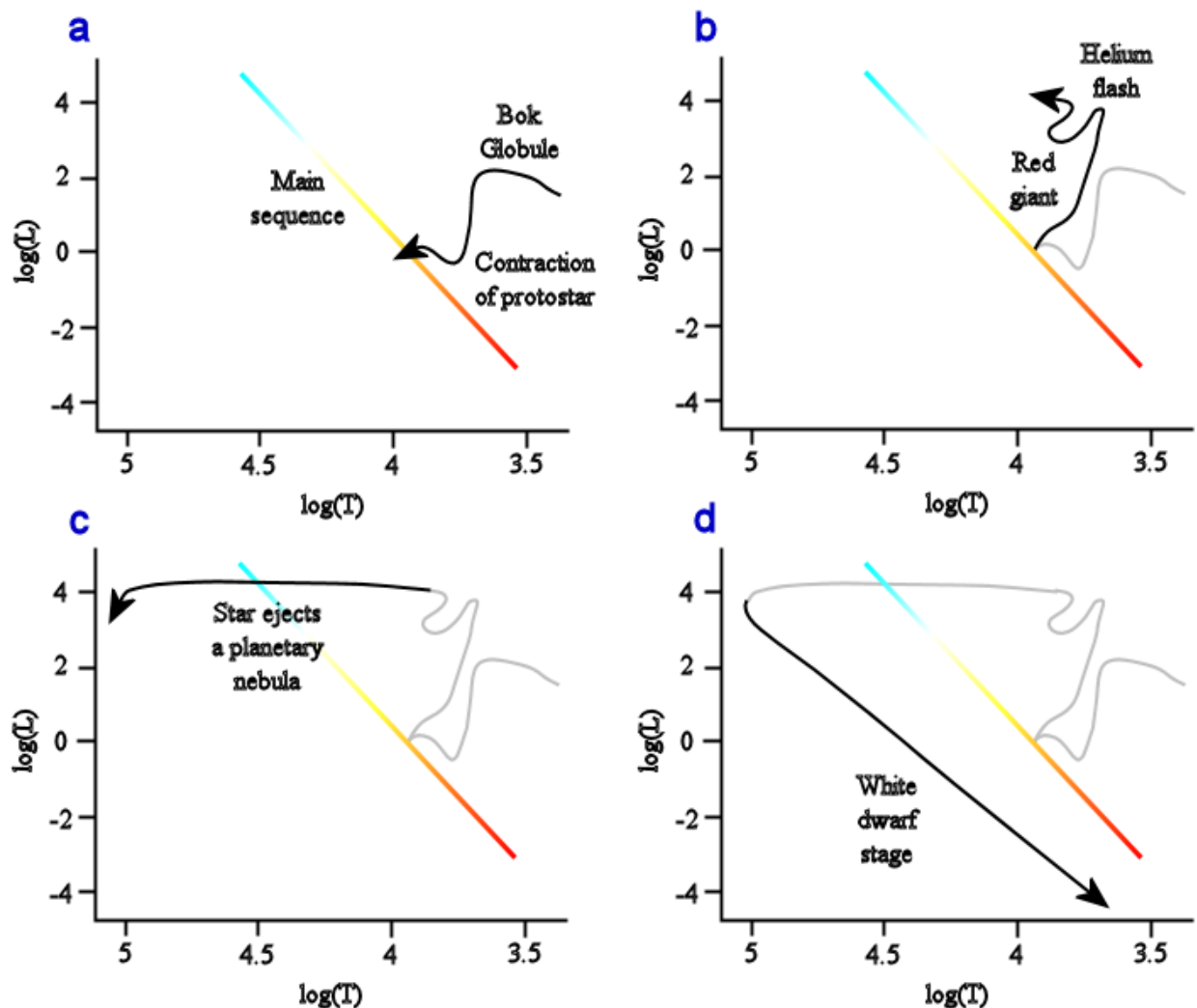


Figure 3.4: Stellar Evolution of Sun-type star: a) Gravitational collapse of a gas cloud forms a protostar which begins to fuse Hydrogen and arrives to the main sequence. b) After billions of years, star leaves the main sequence and becomes a Red Giant. At the tip of the Red Giant branch, star begins to fuse Helium after the episode of Helium flash and slowly moves to AGB phase c) Evolved star expands up to the size of Jupiter's orbit and loses its envelope to form a planetary nebula at the age of 12 billion years. d) Ejecting away the outer envelope, the remnant of dead star shines due to the degeneracy pressure of its electrons and called as White Dwarf. Source: Stars and Nebula by William J. Kaufmann, III

as Chandrasekhar limit.

As per the initial mass of the star, it could reach to three end points of its life - a) White dwarf, b) Neutron star or c) Black Hole. White dwarf is the remnant of a dead star whose core is mainly composed of degenerate matter. At this stage, there is no active nuclear fusion process going inside white dwarfs as there is not enough mass remaining to raise the core temperature for further fusion process. To sustain the system, the electron degeneracy pressure balances the gravitational collapse in White Dwarfs.

If a white dwarf exceeds its mass than 1.44 solar mass, then gravitational pull dominates the electron degeneracy pressure and spontaneous thermal runaway reaction initiates the fusion process

of carbon to heavier elements like neon, oxygen, magnesium, silicon, sulfur, argon, calcium, titanium, chromium, iron to nickel. This process emits an immense amount of energy and the event is called as Type Ia Super Nova, where Ia is the luminosity class. There are other types of super novae (or novae) also occur from different range of masses of stars, however, Type Ia SNe are set as standard candle with absolute luminosity of -19 mag approx. Formation of Neutron star and Black hole results from more massive stars compare to the progenitor of white dwarfs.

3.3 Pulsation of Cepheid

3.3.1 Kappa Mechanism

The kappa mechanism is a key process that drives the pulsations in Cepheid stars.

It operates within the outer layers of the star, specifically in the partially ionized regions where the opacity, represented by the Greek letter kappa (κ), changes significantly with temperature.

The pulsations in Cepheids are characterized by radial expansion and contraction of the outer layers, causing the star to periodically brighten and dim.

The kappa mechanism is responsible for triggering these pulsations by influencing the balance between gravity and radiation pressure in the star's interior.

Opacity and Temperature Sensitivity: Opacity refers to the ability of a medium to absorb and scatter radiation. In Cepheid stars, the opacity is affected by the degree of ionization within the outer layers. At certain temperatures, the opacity experiences a sharp increase, leading to a localized region called the opacity bump.

Expansion and Contraction: During the pulsation cycle, the outer layers of the Cepheid star expand during maximum brightness and contract during minimum brightness. As the star expands, it cools down due to the decrease in temperature. Conversely, during contraction, the temperature increases.

Partial Ionization: As the star expands, the temperature decreases in the outer layers, causing some previously ionized atoms to recombine with electrons, resulting in partial ionization. This ionization state is crucial for the kappa mechanism to operate effectively.

Opacity Bump Effect: Within the partially ionized regions of the Cepheid star, the temperature reaches a point where the opacity is relatively high. This increased opacity affects the balance between gravity and radiation pressure. When the opacity is high, the radiation pressure becomes less effective at counteracting gravity, causing the outer layers to contract.

Energy Transfer: The contraction of the outer layers increases the temperature, reducing the degree of ionization. As a result, the opacity decreases, allowing the radiation pressure to become more efficient. This increased radiation pressure then pushes against gravity, causing the outer layers to

expand.

Feedback Loop: The expansion of the outer layers leads to a decrease in temperature, triggering recombination and an increase in opacity. This increased opacity restricts radiation pressure, causing the outer layers to contract again. This cycle repeats, creating the pulsations observed in Cepheid stars.

3.4 Leavitt Law

To obtain the total luminosity L of a star (total power emitted across all wavelengths and directions), you integrate over the star's entire surface area and over all wavelengths:

$$L = \int_0^{\infty} (4\pi R^2 F_{\lambda}(T)) d\lambda \quad (3.1)$$

$$= 4\pi^2 R^2 \int_0^{\infty} B_{\lambda}(T) d\lambda \quad (3.2)$$

$$= 4\pi R^2 \sigma T^4 \quad (3.3)$$

On plotting a scatter plot in between period and luminosity,a linear relation in between both the parameters with a certain scatter

The period-luminosity relation (also known as the Leavitt Law or the Cepheid period-luminosity relation) is an empirical relationship that exists between the pulsation period and the intrinsic luminosity of Cepheid variable stars. This relationship allows astronomers to determine the distance to Cepheids and calibrate the cosmic distance ladder.

The period-luminosity relation was first discovered by American astronomer Henrietta Leavitt in the early 20th century while studying the brightness variations of Cepheid stars in the Small Magellanic Cloud. Leavitt found that there was a consistent relationship between the periods and the average luminosities of these stars.

The period-luminosity relation states that the longer the period of a Cepheid star's pulsation, the more luminous it is. In other words, there is a direct correlation between the pulsation period and the intrinsic brightness of the star. This relationship allows astronomers to use the observed period of a Cepheid star to determine its intrinsic luminosity.

Once the intrinsic luminosity is known, the apparent brightness (or magnitude) of the star can be measured. By comparing the intrinsic luminosity with the apparent brightness, astronomers can calculate the distance to the Cepheid star using the inverse square law of light.

The period-luminosity relation is valuable because it provides a reliable and relatively straightfor-

ward method for determining distances to Cepheids and, subsequently, to other celestial objects. By measuring the period of a Cepheid star's pulsation, astronomers can estimate its intrinsic luminosity, and from that, they can determine its distance by comparing it to the observed brightness.

The period-luminosity relation has been refined over the years through extensive observations and analysis of Cepheid stars in various galaxies. It has become an essential tool for measuring cosmic distances and has played a vital role in our understanding of the scale of the universe, the expansion rate of the universe (Hubble's Law), and the calibration of other distance indicators, such as Type Ia supernovae.

Part II

Calibration Method and Dataset

4 Calibration Method

4.1 Galactic Cepheid Dataset

The golden data contains photometry with quality index less than or equal to 3 and RUWE less than 1.4 for gaia parallax. Raw dataset contains 103 Galactic Cepheids pulsating in fundamental mode. Their periods are measured in days and scaled logarithmically. The distance modulus is derived from the Gaia DR3 parallax filtered with $\text{RUWE} < 1.4$, the color excess is adopted from Fernie measurements, and photometric magnitudes are collected in the BVIJHK bands. The distribution of each observable against the period is depicted in the following sequence of pair plots. A quick glance shows no clear correlation in the plots.

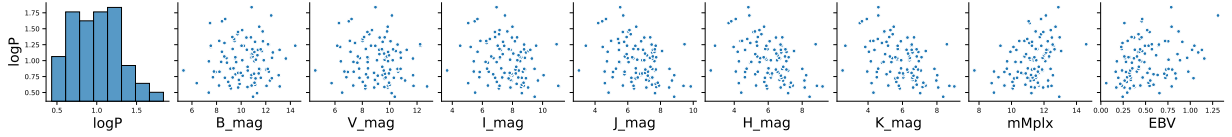


Figure 4.1: 103 Galactic Cepheids BVIJHK photometric data with color excess (E_{BV}) and Gaia distance (RUWE < 1.4). No clear correlation with period is observed in any of the pairplot.

4.2 Leavitt Law and their Wesenheits

Observations in different bands of light provide information about the effect of interstellar reddening on light. For longer wavelengths, the impact of reddening decreases significantly, implying a reduced possibility of reddening errors and leading to a tighter Leavitt Law. In its most generic form, the linear fit to the dataset is expressed as follows:

$$M_\lambda = \alpha_\lambda(\log P - 1) + \beta_\lambda \quad (4.1)$$

$$W_\lambda^{12} = \alpha_\lambda^{12}(\log P - 1) + \beta_\lambda^{12} \quad (4.2)$$

Since the periodic range of Cepheids lies between 0.49 and 1.8 on a logarithmic scale, 1 is chosen as the pivot

Table 4.1: PL relations are shown in six bands, along with the corresponding PW relations in four colors. Notice the decreasing error in the slope and intercept with increasing wavelength.

Band	slope (error)	intercept (error)
M_λ	α_λ	β_λ
B	-1.855 (± 0.110)	-3.221 (± 0.033)
V	-2.259 (± 0.098)	-3.951 (± 0.029)
I	-2.563 (± 0.093)	-4.735 (± 0.028)
J	-2.784 (± 0.088)	-5.218 (± 0.026)
H	-2.917 (± 0.084)	-5.598 (± 0.025)
K	-2.971 (± 0.084)	-5.653 (± 0.025)
Wesenheit	slope (error)	intercept (error)
W_λ	α_λ^{12}	β_λ^{12}
B,BI	-3.175 (± 0.095)	-6.046 (± 0.028)
V,BI	-3.267 (± 0.095)	-6.108 (± 0.028)
I,BI	-3.175 (± 0.095)	-6.046 (± 0.028)
J,BI	-3.078 (± 0.088)	-5.847 (± 0.026)
H,BI	-3.100 (± 0.085)	-5.988 (± 0.025)

point and subtracted from the period before calculating the regression coefficients, i.e., the slope and intercept. The Leavitt Law for each band is shown in Figure 4.8, including four selected Wesenheit variants for VI, VK, IH, and JK.

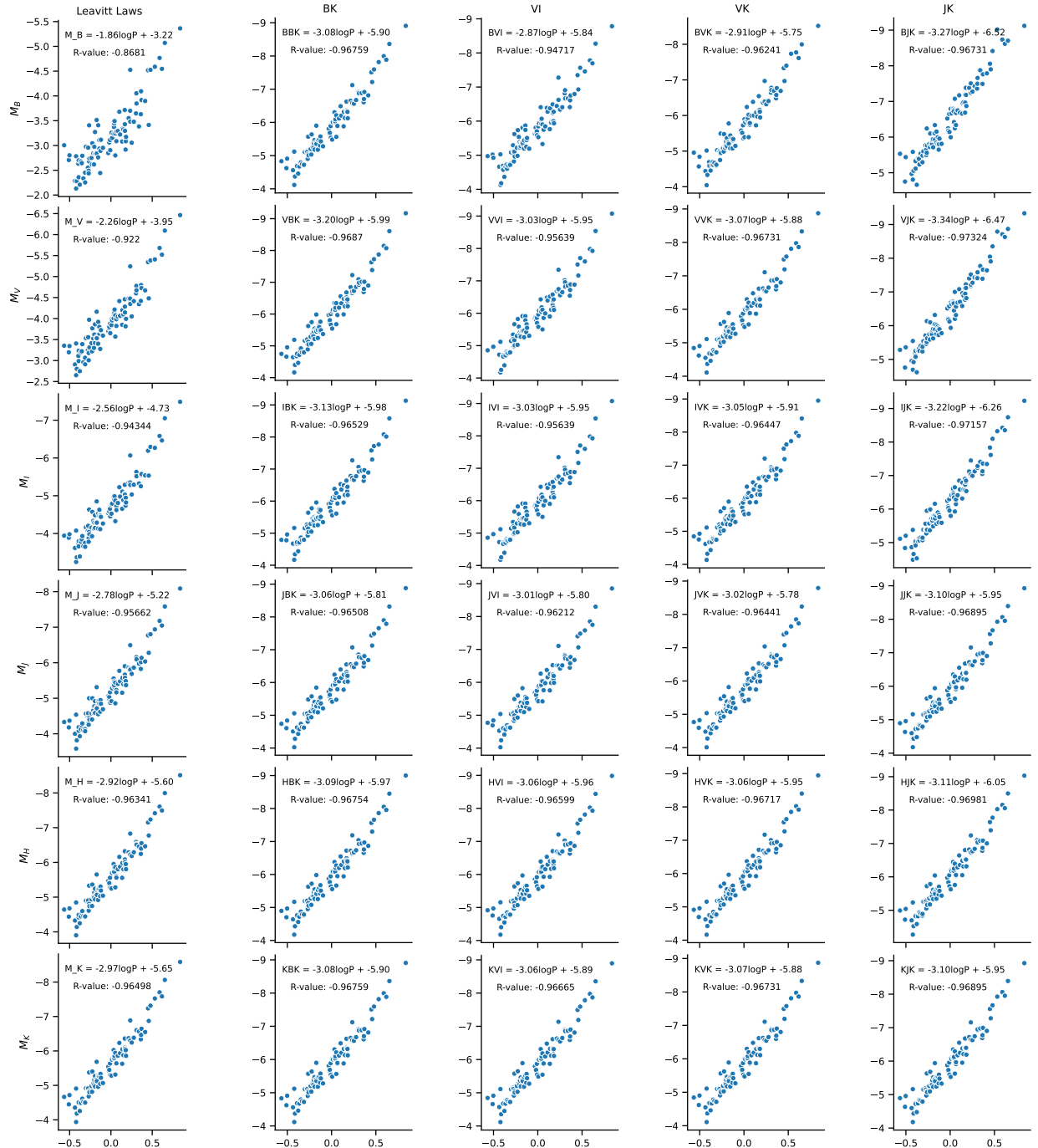


Figure 4.2: BVIJHK PL and PW relations with their Pearson correlation coefficient (r-value).

The plots above provide a comparative overview of the Leavitt Laws across different bands. In the first column,

notice the decreasing width of the PL relation from the B-band to the K-band. The increasing Pearson correlation coefficient indicates a reduction in residuals. Assuming Cepheids align perfectly with the PL relation suggests that the residuals must stem from errors in reddening or distance measurements.

The contribution of residuals due to extinction errors varies with the band, while errors from the distance modulus remain constant. Therefore, the decrease in the width of the PL relation is strongly related to incorrect reddening measurements.

The four variants of the PW relation have relatively higher r-values (approaching -1) than their corresponding PL relations, as Wesenheits are independent of extinction-based errors. Being reddening-free, the scatter in the Wesenheit-based Leavitt Law primarily arises from errors in distance and the reddening ratio. In this research, the reddening ratio is assumed to be correctly known ($R_V = 3.23$, Sandage et al. (2004)), making distance the only source of the scatter.

The slope and intercept of each PL and PW relations are summarized in Table 4.1 and Figure 4.3. The Table 4.1 also list the uncertainty in slope and intercept of PL and PW relation, arising due to a larger scatter. After the calibration, these uncertainty will be diminished significantly.

On the other hand, note the convergence of slope and intercept of PW relations at K band for VI, VK and IH in the adjacent figure. JK based PW relation showing a fine deviation from the rest. These subtle variation in PW slope and intercept suggests a fine-tuning of reddening law for longer wavelength, though such exercise is out of the scope of this thesis. In the next section, procedure for analysing these residual of PL and PW relations is briefly discussed.

4.3 Residual Analysis

The residuals of PL and PW relations are calculated as follows:

$$\Delta M_\lambda = M_\lambda - (\alpha_\lambda \log P + \beta_\lambda) \quad (4.3)$$

$$\Delta W_\lambda^{12} = W_\lambda^{12} - (\alpha_\lambda^{12} \log P + \beta_\lambda^{12}) \quad (4.4)$$

Here, ΔM_λ represents the residuals of the PL relation, and ΔW_λ^{12} represents the residuals of the PW relation. Since distance modulus μ term is involved in both the parameters, M_λ and W_λ , thereby $\delta\mu$, impacts both ΔW and ΔM equally. However, δE_{BV} does not contribute to ΔW , and

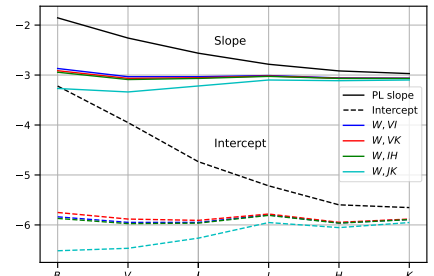


Figure 4.3: Slope and Intercept of BVIJHK PL and PW relations. Interestingly, PW seems constant for all the bands, which is not the case for PL relations.

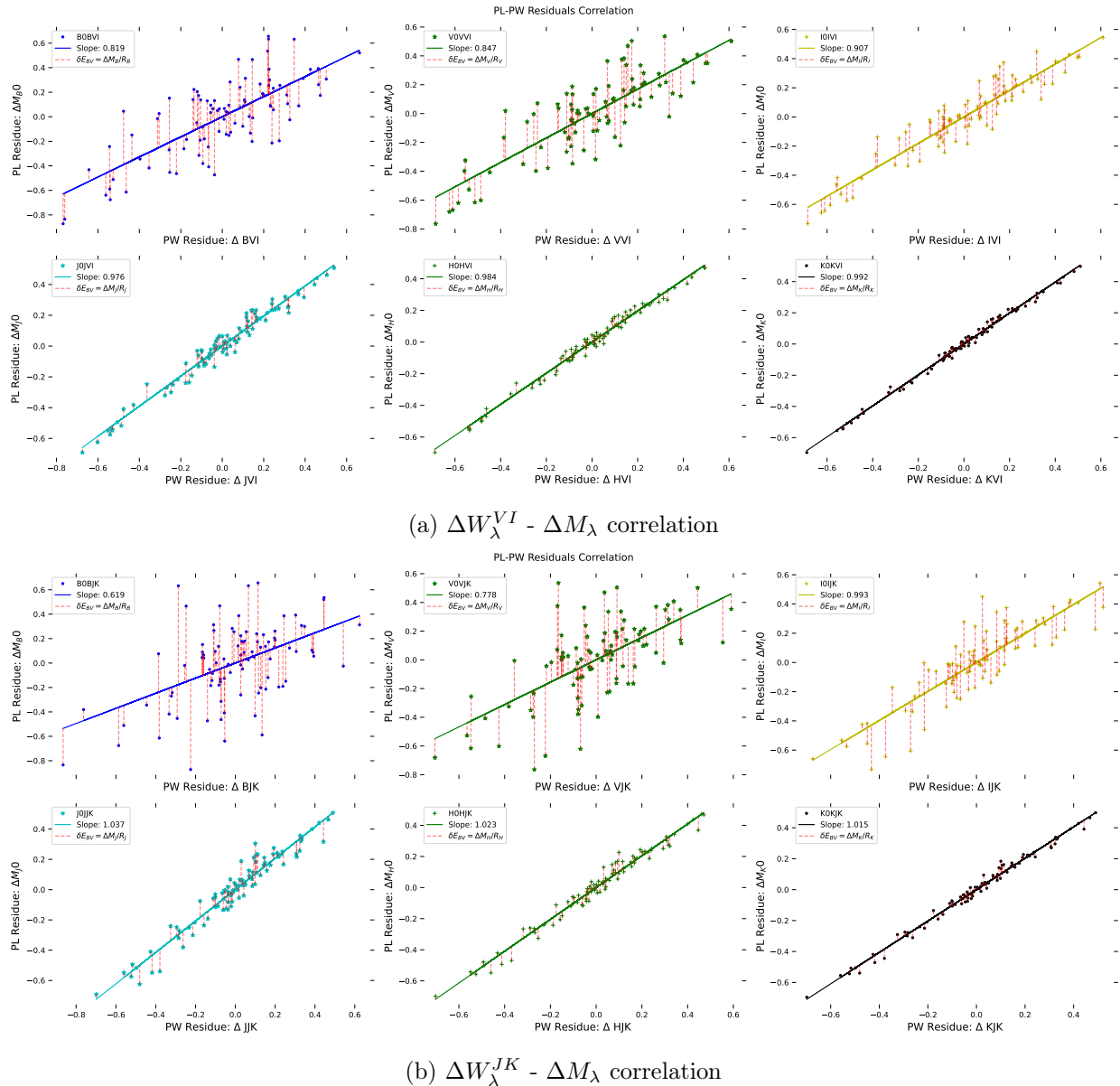


Figure 4.4: $\Delta W - \Delta M$ correlation plots shown for three versions of wesenheit - VI and JK. With increasing wavelength, slope is approaching to 1.

only affects ΔM by an amount of $\delta E_{BV}/R_\lambda = \delta A_\lambda$. Since other possible factor like the effect of metallicity is not considered in this work, the equation for PL and PW residuals, equations 2.27 and 2.28, can be expressed as:

$$\Delta M_\lambda = -(R_\lambda^{BV} * \delta E(B - V) + \delta \mu)$$

$$\Delta W_\lambda^{BV} = -\delta \mu$$

Geometrically, these equations suggest that δE_{BV} (scaled by R_λ^{-1}) shifts a star along the y-axis (vertically), while $\delta \mu$ affects both the x and y axes equally, moving the star along a line with slope 1. For the complete ensemble of stars, the slope of the residual correlation, ρ , when deviating from 1, suggests a significant contribution from reddening errors, as clearly observed for the case of the B and V bands in Figure 4.4. For the longer wavelengths—J, H, and K—the contribution from reddening errors is minimized, and distance-based errors become dominant, causing the slope ρ to approach 1.

Tracing an individual Cepheid in every $\Delta W_\lambda^{12} - \Delta M_\lambda$ correlation plots provides valuable insight into the extinction error associated with each band. By converting the extinction error into reddening error for each band and averaging these values, an estimate of the reddening correction for that specific star is obtained. However, at this stage, the correction for the modulus is not yet determined. To estimate the modulus error, a series of trials for $\delta \mu$ are conducted, which shifts the star along the line of slope 1, as shown in Figure 4.5 for stars B and C. The solid black diagonal line represents the regression line derived from one of the $\Delta W - \Delta M$ plots. The vertical deviation from this regression line, for each trial, reflects the amount of reddening correction needed. Several trial combinations for star B are labeled as 'B0' and 'B1', while 'C2', 'C3', and 'C4' correspond to the trial positions for star C.

These examples illustrate multiple possible error pairs for the B-band. Similar correlation plots are also constructed for the VIJHK bands. Each residual correlation plot provides the corresponding reddening errors for the respective $\delta \mu$ trials, i.e. every $\delta \mu$ trial corresponds to six δE_{BV} . The $\delta \mu$ trial that minimizes the variance of δE_{BV} across the

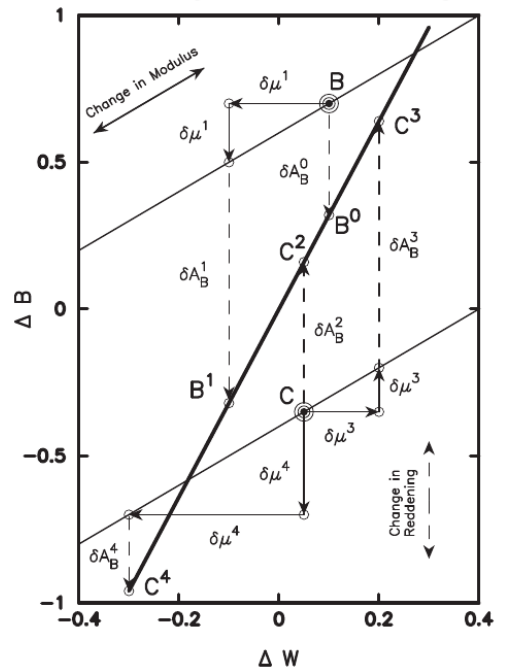


Figure 4.5: For each star, multiple trials are conducted to estimate the reddening-distance error pair in the B band. This process is then repeated for the remaining bands to constrain the correct $\delta \mu - \delta E_{BV}$ error pair. [Madore et al. \(2017\)](#)

bands identifies the correct distance correction trial. This ultimately decouples the error budget between $\delta\mu$ and δE_{BV} for each star.

This method of decoupling errors, introduced by Madore et al. (2017), involves correlating ΔW_V^{VI} with ΔM_λ . In contrast, I have used the composite Wesenheit function, ΔW_λ^{VI} , for each correlation instance. The key motivation behind this choice is the definition of the Wesenheit function, which provides a reddening-free magnitude for the respective band. Specifically, for the VI color, the reddening-free magnitude for the J band should be W_J^{VI} , not W_V^{VI} . This implies that ΔM_J must be correlated with ΔW_J^{VI} . The slopes of the regression lines for the four families of Wesenheit functions—based on BI, VI, IH, and JK—are summarized in Table 4.2.

Band	ρ_λ^{BI} (error)	ρ_λ^{VI} (error)	ρ_λ^{IH} (error)	ρ_λ^{JK} (error)
B	0.797 (± 0.088)	0.819 (± 0.075)	0.791 (± 0.094)	0.619 (± 0.111)
V	0.818 (± 0.066)	0.847 (± 0.060)	0.882 (± 0.079)	0.778 (± 0.095)
I	0.906 (± 0.041)	0.907 (± 0.036)	1.022 (± 0.049)	0.993 (± 0.060)
J	0.979 (± 0.022)	0.976 (± 0.019)	1.013 (± 0.023)	1.037 (± 0.028)
H	0.986 (± 0.014)	0.984 (± 0.013)	1.007 (± 0.015)	1.023 (± 0.018)
K	0.994 (± 0.009)	0.992 (± 0.008)	1.007 (± 0.010)	1.015 (± 0.012)

Table 4.2: Slopes of residual correlation $\Delta W_\lambda^{12} - \Delta M_\lambda$ for BI, VI, IH and JK. Note the systematic decrease in errors as the slope ρ approaching to 1 with increasing wavelength.

4.4 Decoupling $\delta\mu - \delta E_{BV}$

The core process of the calibration is encapsulated in this step. Up until this point, from the Galactic Cepheid dataset, I have derived multiband Leavitt laws and their corresponding Wesenheit Leavitt laws. The correlation of their residuals leads to the results summarized in Table 4.2, which will be used for decoupling the errors δE_{BV} and $\delta\mu$ for each star in the dataset. Given the high sensitivity of reddening at shorter wavelengths, to estimate a realistic correction for reddening error (δE_{BV}), averaging result from the first four bands — B, V, I, and J would be enough.

Since the vertical deviation from the regression line in $\Delta W_\lambda^{12} - \Delta M_\lambda$ suggested the extinction error, mathematically, it can be formulated as:

$$\delta A_\lambda^0 = \Delta M_\lambda - \rho_\lambda^{12} \Delta W_\lambda^{12} - \sigma_\lambda^{12} \quad (4.5)$$

The superscript '0' on A indicates that the distance error trial is not considered yet. ρ_λ^{12} represents the slope of the ΔW_λ^{12} vs. ΔM_λ plot. Since residuals are dispersed around the origin, intercept of the regression lines σ_λ approach to zero and can be neglected.

To convert the extinction error into reddening error, dividing by R_λ^{BV}

$$\delta E^0(B - V)_\lambda = \frac{\delta A_\lambda^0}{R_\lambda^{BV}} \quad (4.6)$$

By making trials for the error in the modulus, $\delta\mu^i$, the corresponding reddening error, δA_λ^i , is calculated as follows:

$$\begin{aligned} \delta A_\lambda(\delta\mu^i) &= (\Delta M_\lambda + \delta\mu^i) - \rho_\lambda^{12}(\Delta W_\lambda^{12} + \delta\mu^i) \\ &= (\Delta M_\lambda - \rho_\lambda^{12}\Delta W_\lambda^{12}) + \delta\mu^i - \rho_\lambda^{12}\delta\mu^i \\ &= \delta A_\lambda^0 + \delta\mu^i - \rho_\lambda^{12}\delta\mu^i \end{aligned}$$

Therefore, for given modulus correction trail, extinction in any band will be calculated as follow:

$$\delta A_\lambda^i = \delta A_\lambda^0 + \delta\mu^i(1 - \rho_\lambda^{12}) \quad (4.7)$$

$$\delta E_\lambda^i(B - V) = \frac{\delta A_\lambda^i}{R_\lambda^{BV}} \quad (4.8)$$

$$(4.9)$$

Considering ideal case where extinction law $\frac{A_\lambda}{A_V}$ and reddening ratio R_λ are precisely known for the line-of-sight of each Cepheid of the dataset. Let i number of trails made for modulus correction $\delta\mu$ which correspond to six variants of reddening corrections (BVIJHK) for each wesenhheit-color (BI, VI, IH and JK). Each Cepheid yields an error matrix of 100 rows ($\delta\mu^i$) and 6 x 4 columns for expected $\delta E_\lambda^i(B - V)$.

Let, k^{th} trail be the correct one, i.e. reddening corrections δE_λ suggested by each band must be agreeing with remaining ones., $\delta\mu^k$ must yield the same reddening correction δE^k for all the bands, implying their variance is zero.

$$\delta E_{BV}(\delta\mu^k) = \delta E_B^k = \delta E_V^k = \delta E_I^k = \delta E_J^k = \delta E_H^k = \delta E_K^k = \langle \delta E_\lambda^k \rangle_\lambda \quad (4.10)$$

For dataset, it the variance across the bands being the minimum for the best solution, when .

$$k = \min(\text{var}(\delta E_\lambda^i(B - V))_\lambda)_i \quad (4.11)$$

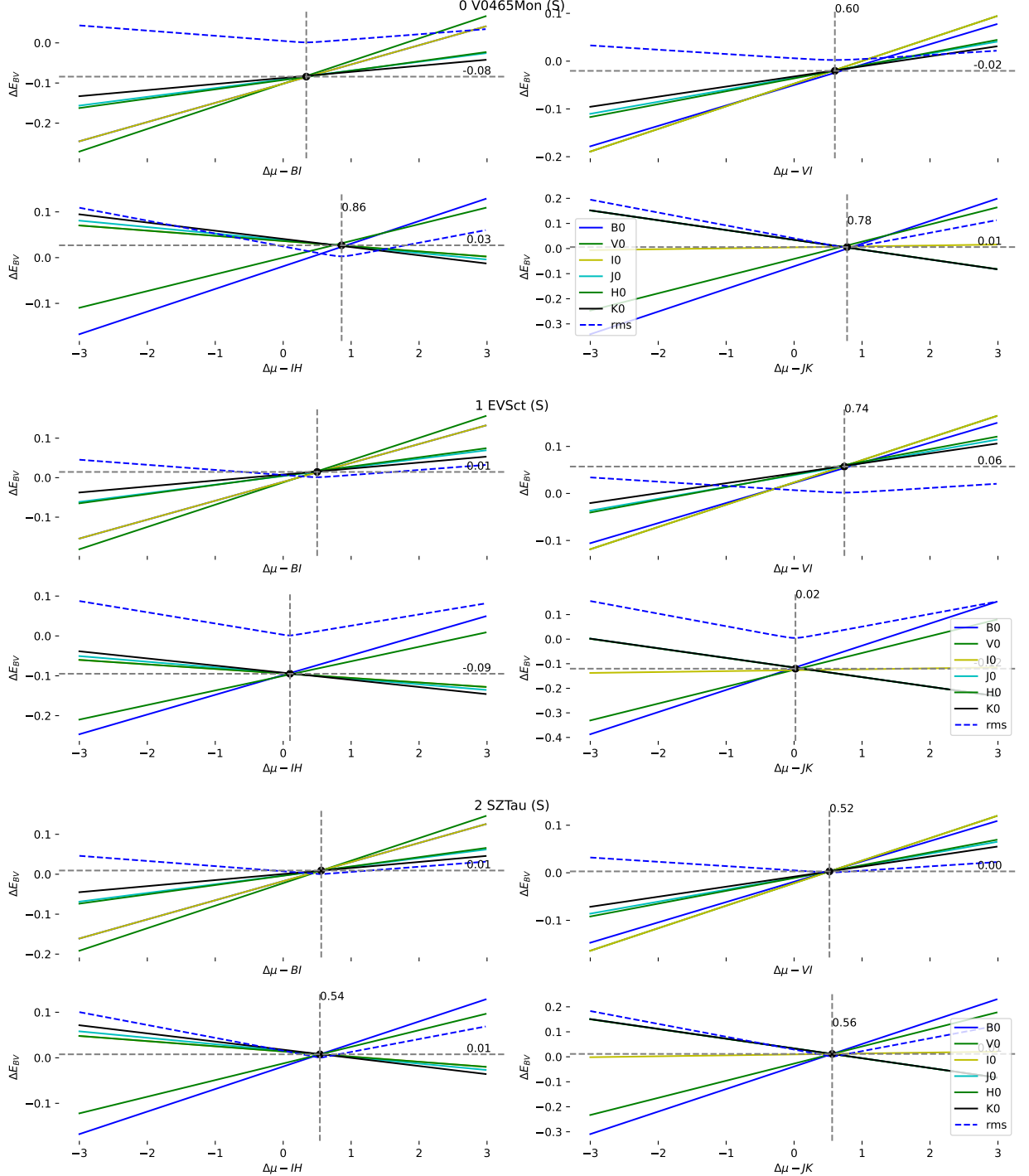


Figure 4.6: Determination of reddening error with least variance over modulus error for four family of wesenheit function. Dashed blue line dipects the variance.

4.5 Calibrated Leavitt Law

These corrections will be adjusted with the original data as follow.

$$M_{\lambda}^* = M_{\lambda}^0 + \delta A_{\lambda}^* + \delta \mu^*$$

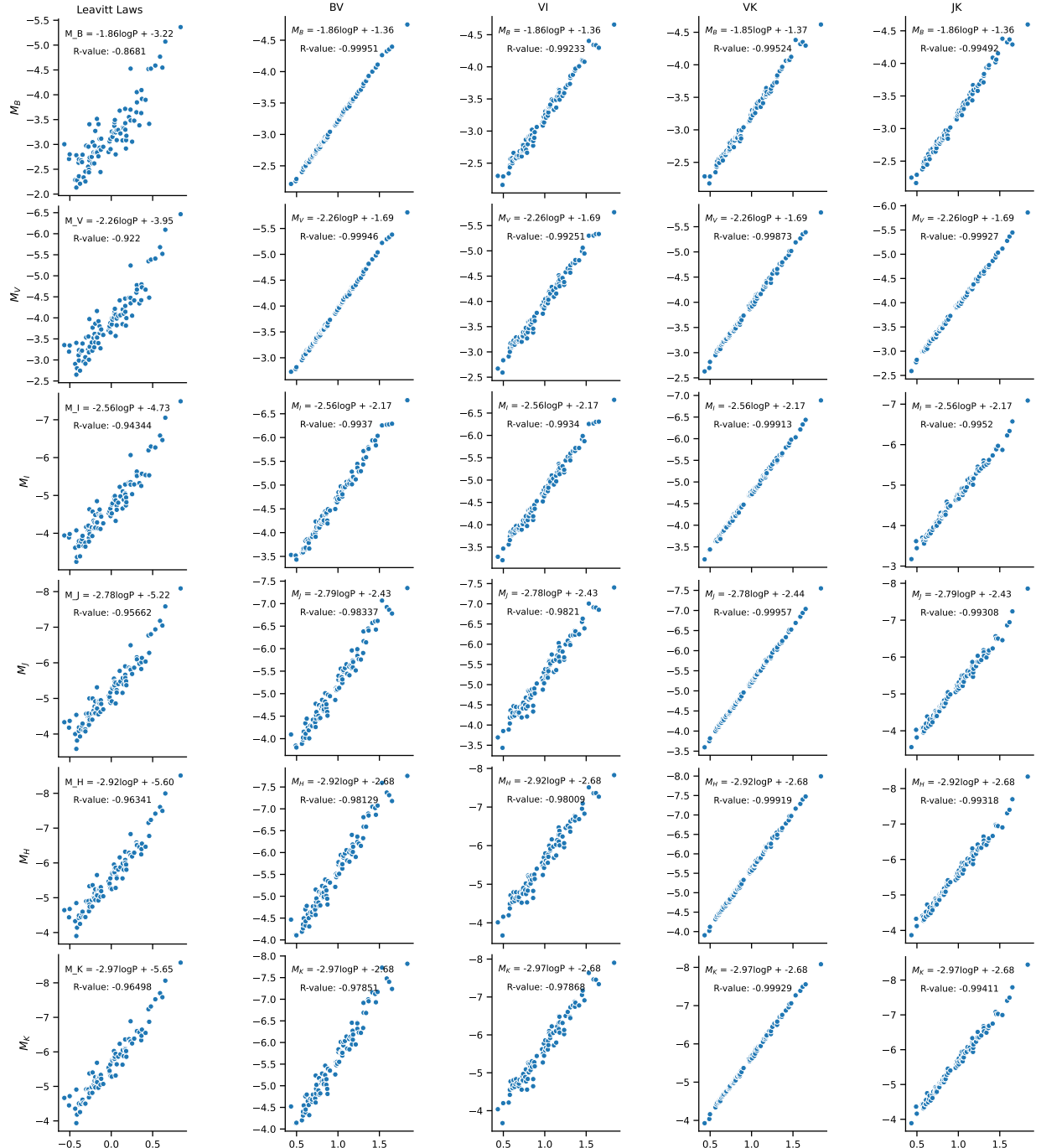


Figure 4.7: BVIJHK PL and PW relations with their Pearson correlation coefficient (r-value).

4.6 cluster Cepheid

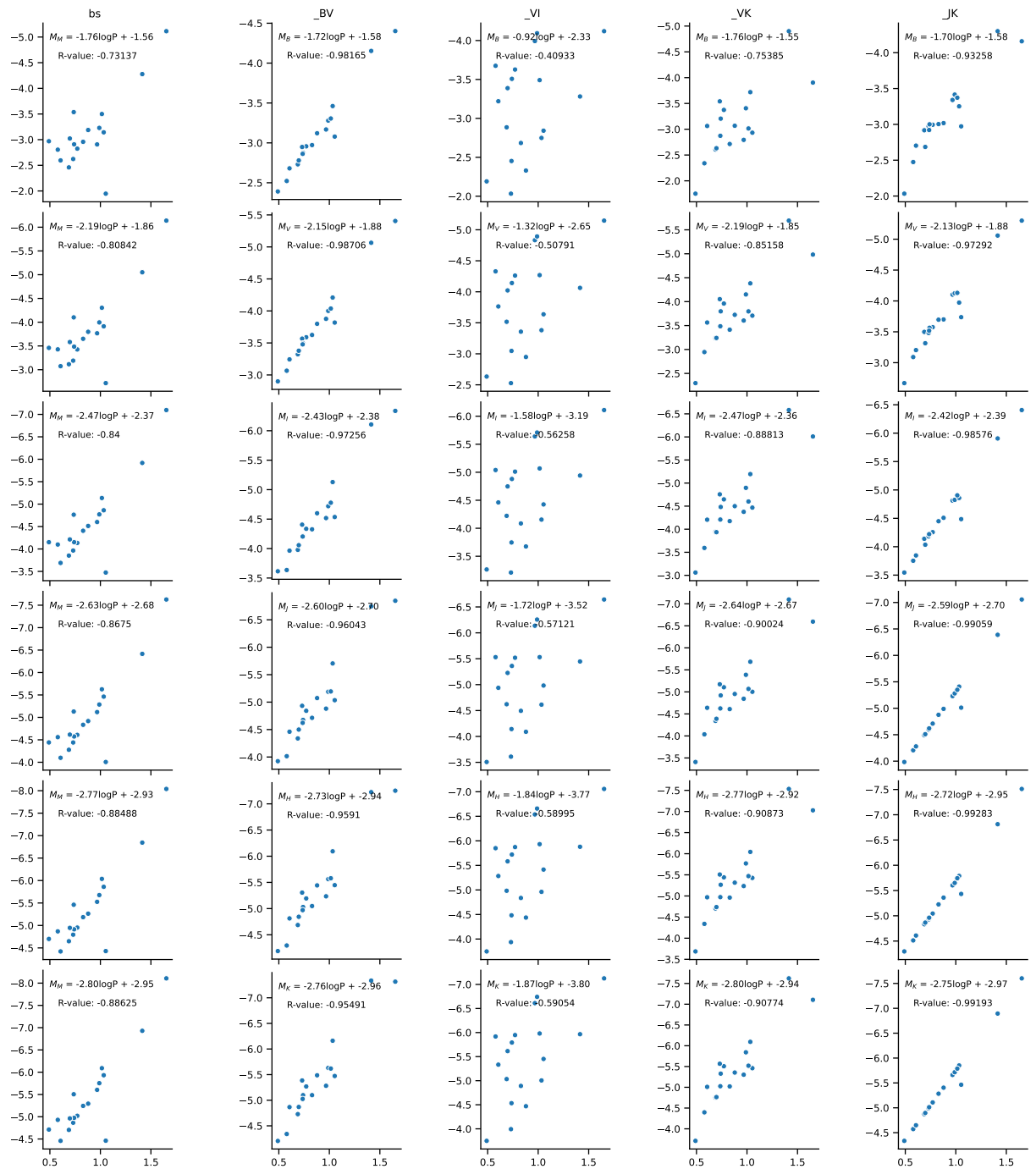


Figure 4.8: BVIJHK PL and PW relations with their Pearson correlation coefficient (r-value).

5 Discussion

5.1 Reddening Comparison

?

5.2 Distance Comparison

5.3 Luminosity Comparison

5.4 Effect of Metallicity

?

6 Conclusion

6.1 Result

6.2 Application Of The Result

Appendix

Appendix

Mathematical Tools

Linear Regression

sda

Baade-wesselink method

linetocchapterAppendix

Bibliography

- Akrami, Y., Ashdown, M., and Aumont, J. (2020). Planck2018 results: VII. isotropy and statistics of the cmb. *Astronomy & Astrophysics*, 641:A7.
- Alpher, R. A. and Herman, R. (1948). Evolution of the universe. *Nature*, 162(4124):774–775.
- Baade, W. (1958). Problems in the determination of the distance of galaxies. *The Astronomical Journal*, 63:207–210.
- Bethe, H. A. (1939). Energy production in stars. *Physical Review*, 55(5):434.
- Cardelli, J. A., Clayton, G. C., and Mathis, J. S. (1989). The relationship between infrared, optical, and ultraviolet extinction. *The Astrophysical Journal*, 345:245–256.
- Eddington, A. (1920). The internal constitution of the stars. *The Scientific Monthly*, 11(4):297–303.
- Eddington, A. S. (1917). The pulsation theory of Cepheid variables. *The Observatory*, 40:290–293.
- Einstein, A. (1917). Kosmologische betrachtungen zur allgemeinen relativitätstheorie. *Sitzungsberichte der Königlich Preussischen Akademie der Wissenschaften*, pages 142–152.
- Fernie, J. (1994). Color excesses for classical cepheids from bv photometry. *The Astrophysical Journal*, vol. 429, no. 2, pt. 1, p. 844-845, 429:844–845.
- Fouqué, P., Arriagada, P., Storm, J., Barnes, T., Nardetto, N., Mérand, A., Kervella, P., Gieren, W., Bersier, D., Benedict, G., et al. (2007). A new calibration of galactic cepheid period-luminosity relations from b to k bands, and a comparison to lmc relations. *Astronomy & Astrophysics*, 476(1):73–81.
- Freedman, W. L. (2021). Measurements of the hubble constant: tensions in perspective. *The Astrophysical Journal*, 919(1):16.
- Gamow, G. (1948). The evolution of the universe. *Nature*, 162(4122):680–682.
- Hubble, E. (1925). Cepheids in spiral nebulae. *The Observatory*, 48:139–142.
- Hubble, E. (1929). A relation between distance and radial velocity among extra-galactic nebulae. *Proceedings of the national academy of sciences*, 15(3):168–173.

- Johnson, H. L. and Morgan, W. W. (1953). Fundamental stellar photometry for standards of spectral type on the revised system of the yerkes spectral atlas. *The Astrophysical Journal*, 117(3):313–352.
- Krelowski, J. and Papaj, J. (1993). The interstellar extinction curve. *Publications of the Astronomical Society of the Pacific*, 105(693):1209.
- Leavitt, H. S. (1908). 1777 variables in the magellanic clouds. *Annals of Harvard College Observatory*, 60(4):87–103.
- Leavitt, H. S. and Pickering, E. C. (1912). Periods of 25 variable stars in the small magellanic cloud. *Harvard College Observatory Circular, vol. 173, pp. 1-3*, 173:1–3.
- Lemaître, A. G. (1931). Contributions to a british association discussion on the evolution of the universe. *Nature*, 128(3234):704–706.
- Madore, B. (1982). The period-luminosity relation. iv-intrinsic relations and reddenings for the large magellanic cloud cepheids. *The astrophysical journal*, 253:575–579.
- Madore, B. F., Freedman, W. L., and Moak, S. (2017). A method for improving galactic cepheid reddening and distances. *The Astrophysical Journal*, 842(1):42.
- Payne-Gaposchkin, C. H. (1925). *Stellar atmospheres: A contribution to the observational study of high temperature in the reversing layers of stars*. PhD thesis, Radcliffe College, United States.
- Penzias, A. A. and Wilson, R. W. (1965). A Measurement of Excess Antenna Temperature at 4080 Mc/s. *The Astrophysical Journal*, 142:419–421.
- Planck, M. (1900). On the theory of the energy distribution law of the normal spectrum. *Verh. Deut. Phys. Ges*, 2(237):237–245.
- Riess, A. G. and Filippenko, A. V. (1998). Observational Evidence from Supernovae for an Accelerating Universe and a Cosmological Constant. *Astrophysical journal*, 116(3):1009–1038.
- Riess, A. G., Yuan, W., Macri, L. M., Scolnic, D., Brout, D., Casertano, S., Jones, D. O., Murakami, Y., Anand, G. S., Breuval, L., et al. (2022). A comprehensive measurement of the local value of the hubble constant with 1 km s⁻¹ mpc⁻¹ uncertainty from the hubble space telescope and the sh0es team. *The Astrophysical Journal Letters*, 934(1):L7.
- Sandage, A. (1958). Current problems in the extragalactic distance scale. *The Astrophysical Journal*, 127:513.
- Sandage, A., Tammann, G., and Reindl, B. (2004). New period-luminosity and period-color relations of classical cepheids-ii. cepheids in lmc. *Astronomy & Astrophysics*, 424(1):43–71.

Storm, J., Gieren, W., Fouque, P., Barnes, T. G., Pietrzyński, G., Nardetto, N., Weber, M., Granzer, T., and Strassmeier, K. (2011). Calibrating the cepheid period-luminosity relation from the infrared surface brightness technique-i. the p-factor, the milky way relations, and a universal k-band relation. *Astronomy & Astrophysics*, 534:A94.

Whiteoak, J. B. (1966). The Wavelength Dependence of Interstellar Extinction. *The Astrophysical Journal*, 144:305.